Optical Properties of Cancrinite

Tinja Kylänpää
Master’s thesis
Intelligent Materials Chemistry
Department of Chemistry
University of Turku
April 2026

Subject: Chemistry
Author: Tinja Kylänpää
Title: Optical Properties of Cancrinite
Supervisors: Bettiina Muurinen, Pinja Tamminen, Natalia Antonova, Anssi Peuronen, Mika Lastusaari
Number of pages: 46 pages
Date: April 2026

Cancrinite ($Na_8Al_6Si_6O_{24}(OH)_2 \cdot H_2O$) is an aluminosilicate mineral with an ordered framework of 6- and 12-memebered rings which form a porous network structure. These pores can host e.g. CO_3^{2-}, OH^-, Cl^-, SO_4^{2-} anions and K^+, Ca^{2+}, Cs^+ cations which can cause optical properties in cancrinite. The most common route for cancrinite preparation is hydrothermal synthesis using Teflon-lined steel-autoclaves in alkaline media to create the needed dissolution for crystallisation. The synthesis has been optimised for several different applications, some of which include pigment development, radioactive waste management, and photonic crystals. Cancrinite readily accepts several different ions, but the recent studies have focused more on the naturally occurring cancrinite or entrapment of radioactive ions. Most properties of cancrinite are still uncovered, since the research on it has been scarce. This thesis aims to explore the photochromic and luminescent properties of cancrinite.

In this research, cancrinite samples with various anions and cations were synthesised. Each sample batch, named by their cation(s), were characterised by powder X-ray diffraction, X-ray fluorescence spectroscopy, as well as diffuse reflectance and photoluminescence spectroscopies. Additionally, field emission scanning electron microscopy combined with energy-dispersive X-ray spectroscopy, thermoluminescence, and optically stimulated luminescence measurements were carried out of the samples that excelled in their properties. Depending on the results of thermoluminescence and optically stimulated luminescence, possible dental X-ray image could be obtained.

The results showed that cancrinite readily accepted ions creating colour and luminescence centres with certain samples showing better properties. While the properties of cancrinite are not comparable to the properties of sodalites, these properties reveal more about the mechanisms of cancrinite-group minerals.

Keywords: cancrinite, ion substitution, photochromism, luminescence

Abbreviations

BMS = Barium magnesium silicate ($BaMgSiO_4$)

CAN = Cancrinite

EDS = Energy-dispersive X-ray spectroscopy

ESR = Electron spin resonance

FE-SEM = Scanning electron microscope

IR = Infrared

NIR = Near-infrared

PeL = Persistence luminescence

PL = Photoluminescence

TL = Thermoluminescence

TT = Thermotenebrescence

UV = Ultraviolet

XRD = X-ray diffraction

XRF = X-ray fluorescence

1 Introduction

1.1 Cancrinite

Cancrinite ($Na_8Al_6Si_6O_{24}(OH)_2 \cdot 2H_2O$ for basic cancrinite) is a microporous hexagonal compound. It has ordered framework that forms of layered 6-membered AlO_4 and SiO_4 tetrahedral units (**Figure 1**).[1] The characteristic structure of cancrinite is formed of ε-cages that consists of five 6-membered rings and six 4-membered rings.[2] These two types of rings form a large continuous channel that consists of 12-membered rings creating the space group of $P6_3$.[1–4] The large pore size of the 12-membered rings (~5.9 Å) enables cancrinite to host both cations and anions, while the ε-cages are smaller (~2.2 Å) and can only accommodate cations and/or water molecules. The cages and the channels are charged negatively in the framework which can be neutralised by extra-framework cations entering the structure of the porous material. Under mild hydrothermal synthesis conditions, anionic extra-framework species can be clathrated in the structure during its formation.[1,4]

Despite cancrinite belonging to feldspathoid mineral group, due to structure it can be considered a zeolite-type material and a molecular sieve.[4,5] Cancrinites resemble sodalite structure with its aluminosilicate framework which can easily lead to the transformation to the cubic sodalite structure, e.g. to nosean ($Na_8(Al_6Si_6O_{24})(SO_4) \cdot H_2O$).[1]

In nature, cancrinite is a relatively common mineral[6] appearing white, light blue, grey, greenish, yellowish or bright yellow.[5] Cancrinite forms under alkaline environment and high CO_2 pressure either as a primary mineral or a secondary product of nepheline in alkaline-rich igneous rocks.[7,8] Cancrinite, named after by Count Georg Ludwig Cancrin, was found in 1839. In 1930, Pauling[9] proposed the first crystal structure for cancrinite and in 1965, Jarchow refined the structure further.[8]

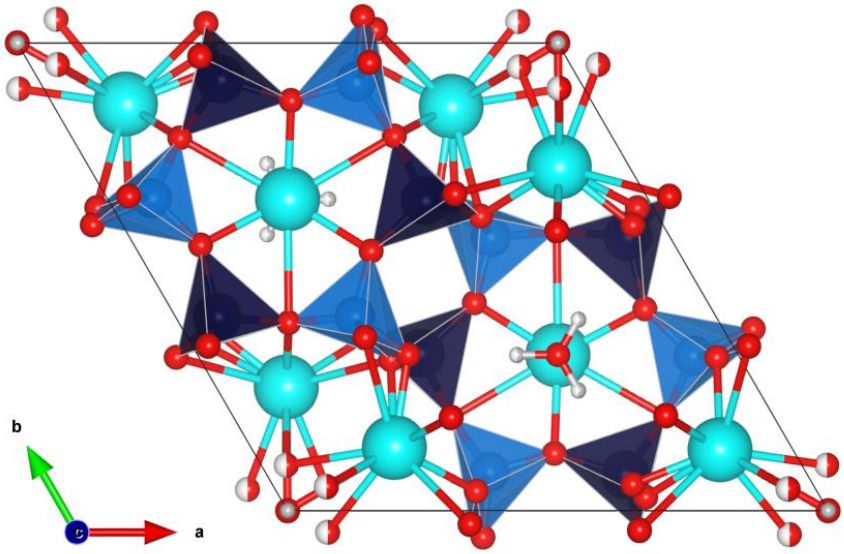

Figure 1. Unit cell of basic cancrinite. The AlO_4 and SiO_4 tetrahedra are represented in dark blue and light blue, respectively. Na atoms are cyan, while H atoms are grey. The partial white colouring of the red O atoms represents partial occupancy.

1.2 Synthesis methods of cancrinite

The most common synthesis route for cancrinite is hydrothermal synthesis using a Teflon-lined stainless-steel autoclave. The source of aluminosilicate precursor typically is either sodium aluminosilicate gels or zeolitic clays, such as kaolin.[1,10–13] In many cases, the synthesis is done in alkaline solution with the concentration varying from 2 to 16 M. The basicity is controlled with the amount of NaOH, which often gets mixed together with 1-2 g of kaolin. Up until recently, different variations of nitrite and carbonate cancrinite were synthesised with different crystallisation times with the shortest being 10 h and the longest 120 h.[11] Although, most often the synthesis times of 24 or 48 h are used.[1,10,12] The synthesis temperature varies from 80 to 220 °C.[12,13] After which, the resulting product can be filtered and washed with distilled water followed by drying in 80 °C.[11,12]

With the basic cancrinite synthesis procedure, many variations of cancrinite can be synthesised. Weller and Kenyon[12] synthesised deuterated carbonate cancrinite by replacing the H_2O molecules with D_2O. In that work, the synthesis temperature differed from most and 220 °C was used, after which the wash completed using D_2O. Additionally to the deuteration of cancrinite, they also performed temperature tests, which revealed the decomposition of the hydrogenous samples. The water molecules located in 6-memebered channels would get released at temperatures 100-250 °C which causes the Na^+ atoms to reposition. Above 500-600 °C, nepheline ($Na_3K(Al_4Si_4O_{16})$) started forming due to the decomposition of the structure.[12]

Cancrinite synthesis and formation can happen via other routes as well. It has been found that cancrinite precipitates from sludge tanks[7,14] and can be synthesised from coal gangues via uniform paste[15].

1.3 Ion substitution in cancrinite

Due to the highly porous structure, cancrinite has been considered useful for pigment development[16], radioactive waste management[7,15,17], photochemistry[18], and photonic crystals[19]. The properties of cancrinite can be tuned by introducing different cationic and anionic components in the channel voids to suit each application.[5] The most common anions are CO_3^{2-}, OH^-, NO_3^-, Cl^- and SO_4^{2-}.[2,20] The cationic component is usually Na^+, but some amounts can be substituted to K^+, Ca^{2+}, Li^+, and Cs^+.[5,21,22]

The distribution and ratios of extra-framework elements, i.e. cations, anions, and H_2O, have been explored in a study done by Pekov et al.[23] In the cationic composition, Na dominates over K or Ca in all cancrinite subgroup minerals, but in cancrinite, Ca is prevalent. The sulphate-rich minerals in the subgroup are more prone to have K in the structure, while having diminishing amounts of Ca. This also means that Ca-rich minerals are lacking K. In addition, it has been indicated that sulphate strongly stays in the cancrinite-type materials.[23] Importantly, Pekov et al. also studied correlations between S and Cl in the cancrinite subgroup, and found the minerals severely depleted of Cl. They theorised that inclusion of Cl is due to small amounts of sodalite.

One example of using cancrinite in radioactive waste management is using it to trap Sr^{2+} ions. Wang et al.[15] explored immobilising Sr during nuclear leakage incident using coal gangue as the precursor. They concluded that the Sr^{2+} ions were able to enter the structure of cancrinite, but the quantity is heavily reliant on the anion content of added salt. They also noticed that cation content over 25% of the overall cation content led to the alkali activator effectiveness decreasing.[15] In another study done by Buck and McNamara[7], nitrite-cancrinite with ^{137}Cs ions was found in high-level waste tank sludge. Through their experiments, they noticed cancrinite formed twinning of platy crystals which were able to incorporate ^{137}Cs in them. They also concluded that the cancrinite formed in the tanks was identical to synthesised cancrinite.

Similar study was done on cancrinite and sodalite forming in the same high-level waste tank by Deng et al.[14] They investigated how Cs^+, K^+, Sr^{2+}, Ca^{2+}, and Mg^{2+} affected the transformation pathways and crystallinity of these two minerals. The result of the study was that the crystallinity improved in the presence Cs^+ and Sr^{2+} ions. The effect of the cations on cancrinite formation was minimal at high NaOH concentrations but the cause for this minimal

effect could be the competition produced by Na^+ ions.[14] On top of these ions, Pb has been encapsulated in cancrinite along with S^{2-} ions. A paper by Miyake et al.[24] explored this possibility by synthesising sulphide-cancrinite with the conclusion that the Pb^{2+} ions were found in the 12-membered ring with S^{2-} ions instead of replacing Na^+ ions.

1.4 Photochromism in cancrinite

Photochromism, also known as tenebrescence among mineralogists, is a reversible colour change induced by electromagnetic radiation in the X-ray, UV, and visible ranges.[25–27] The colour change happens due to the structural or electronic state changes.[26] The reverse reaction can occur by heating, chemical oxidation or exposure to the light at different wavelengths.[27]

Photochromism in cancrinite has been observed when it contains carbonate anions as the main anionic compound, since X-ray or UV irradiation can lead to formation of carbonate hole radicals.[5,28] Shendrik et al.[5] investigated on $CO_3^{\bullet-}$ hole radical formation in cancrinite samples by irradiating it with X-rays leading to the sample turning blue (**Figure 2**). Chukanov et al.[20] noticed the same phenomenon regarding to $CO_3^{\bullet-}$ radicals. Using ESR (electron spin resonance) measurements, they concluded that the blue colour comes from $CO_3^{\bullet-}$ hole radical anions. They also measured UV-Vis-NIR absorption spectrum which showed intense absorption band at ~621 nm and in the range of 270-400 nm.[20] In addition, both Shendrik et al.[5] and Chukanov et al.[20] found that $S_3^{\bullet-}$ radicals caused the yellow-blue colour of the synthetic material which is partly at fault for the absorption bands. Hoffman et al.[16] also have studied the $S_3^{\bullet-}$ radicals which can be incorporated into the ε-cages of cancrinite. They found that $S_3^{\bullet-}$ and $S_2^{\bullet-}$ act as blue and yellow chromophores in cancrinite structure, respectively. [29]

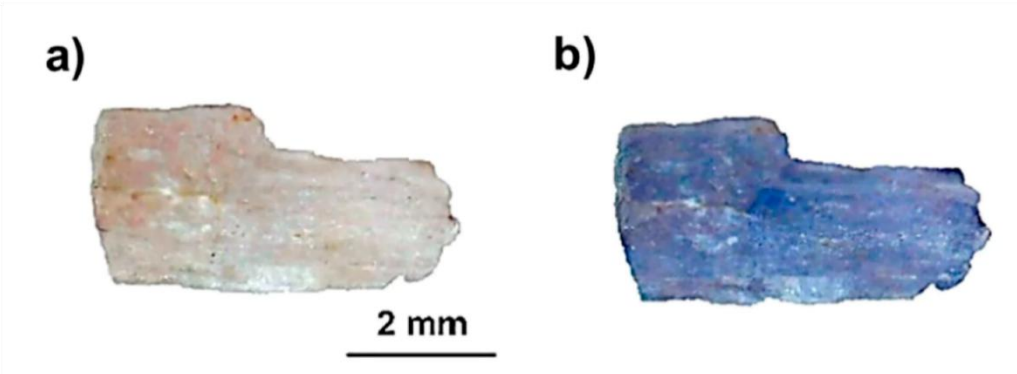

Figure 2. Cancrinite sample a) before and b) after 10^4 Gy irradiation. Figure adapted from Fig 6. in Ref by Shendrik et al., **11**, (2021).[5]

The mechanism for photochromic sodalite, hackmanite, is based on the colour centres which trap electrons in defect energy levels in the bandgap.[30] For hackmanite, photochromism originates from having a sulphur impurity, where Cl^- gets replaced by S_2^{2-}. This creates a Cl

vacancy. By irradiation, the S_2^{2-} impurity loses one electron to the Cl vacancy, which leads to the electron getting trapped in a colour centre.[25,30] It has been established that the colour centres present in hackmanite, F-centres, are metastable due to their ability release electrons back to the sulphide anions by heating or under visible light.[30] This leads the material to return to its original colour.[30] Other mechanisms are also known, such as photochromism activating by redox reaction. A material, using redox reaction as the mechanism, causing large photochromic contrast is Fe-doped $BaMgSiO_4$ (BMS). The mechanism is reliant on the reduction and oxidation of the iron ions.[29]

The photochromism of sodalites has been researched intensely with the most common chloride variation, but also with other salts, which led to the findings of how each ion affects photochromism (**Table 1**). Due to cancrinite and sodalite being closely related minerals, they may share optical properties and their mechanisms. The likelihood of replicating the effects of the different ions is strong, since research shows that cancrinite readily accepts many ions.

Table 1. How some ions can affect the photochromism in sodalites listed.

Substituted element	Substituted with	Effect of the substituted element
Na	K	Lowered activation energy[25] Broadened absorption band[31]
Na	Li	Absorption wavelength shifts to longer wavelengths[32] Weakens photochromism[33]
Cl	S	Increasing the amount of S slows the bleaching rate[34]
Cl	Br, I	Colouration and fading rates increase[34] Absorption wavelength shifts to longer wavelengths[32,35] Larger unit cell[32,35]
Cl	F	Colouration and fading rates decrease[34]

1.5 Luminescence in cancrinite and similar materials

Many minerals with aluminosilicate framework exhibit luminescence, e.g. sodalite ($Na_8Al_6Si_6O_{24}(Cl,S)_2$)[33,36], nepheline ($Na_3K(Al_4Si_4O_{16})$)[37,38], and kyanoxalite ($Na_7(Al_{6\text{-}6.5}Si_{6\text{-}6.5}O_{24})(C_2O_4)_{0.5\text{-}1}\cdot 5H_2O$)[20,39]. Numerous silicate minerals have UV emission caused by Si–O bonding defects or non-bridging oxygen or silicon vacancy-hole centres. The stressed Si–O bonds in the 3D lattices of tectosilicate minerals, e.g. quartz, zeolites, scapolites, are the cause

for the emission.[40] Many of these minerals can be found as S-bearing in nature with chromophore and luminescent centres being $S_3^{\bullet-}$ and $S_2^{\bullet-}$, respectively.[39]

In many S-bearing feldspathoids, the SO_4^{2-} anion and $S_3^{\bullet-}$ radical anion are stable at high temperatures in oxidising atmosphere. However, these ions transform into S^{2-}, HS^-, $S_4^{\bullet-}$, $S_2^{\bullet-}$, S_4 or mixture of these. Some of these ions along with $S_3^{\bullet-}$ and S_5^{2-} are responsible for colour centres in these materials. Emission caused by UV irradiation is, presumably, due to $S_2^{\bullet-}$, Fe^{3+}, and their combinations.[41]

The luminescence properties of cancrinite itself have not been well researched, but some studies show cancrinite having luminescence. In 2021 Kaneva and Shendrik[28] found intrinsic luminescence in cancrinite as a result of CO_3^{2-} anion forming $CO_3^{\bullet-}$ radicals under UV or X-ray irradiation at temperatures above 150 K. Whereas at temperatures below 150 K, the luminescence was caused by the radiative recombination of electronic excitations close to oxygen atoms.

It has also been reported that kaolin, the most common precursor of cancrinite, can have luminescence properties upon UV irradiation. Ouarab et al.[42] experimented adding $AlPO_4$ nanocrystals into the structure to achieve high sensitivity to UV irradiation. They successfully attained high-intensity emission primarily caused by PO_4^{3-} ions but also noticed that oxygen and hydroxyl vacancies enhanced the emission. These vacancies could carry on to the structure of cancrinite influencing the emission produced by cancrinite.

1.6 Aims of this work

The photochromism and luminescent properties of cancrinites have not been researched extensively, which this work aims to explore. The need for better and more sustainable materials has increased which is why researching of different materials is essential. If sodium and the extra-framework anion can be substituted to different ions in the cancrinite framework while creating similar properties to photochromic and luminescent sodalites, it could deepen the understanding of the optical mechanisms involved. Cancrinite could expand the applications meant for sodalites, but with different colour change properties and excitation and emission wavelengths. This way the knowledge could be expanded to other mineral groups and more properties could be discovered.

The starting point of this project is to see if disulphide ions and chloride vacancies act as colour centres in cancrinite, which should allow photochromic properties to take place. This was done by replacing some of the sulphate ions in sulphate cancrinite (SO_4-CAN) with chloride, and later, with other anions. The substitutions were expanded to cations as well.

Cancrinite is already known to exhibit optical properties when containing certain extra-framework anions or cations, but this research is another step towards understanding cancrinite and harnessing its full utility.

2 Experimental Section

2.1 Synthesis of the substituted cancrinite

The cancrinite samples were synthesised using method based on the work of Buhl J. et al. 2019, in which they used kaolin as the Si-Al source. The hydrothermal synthesis required 20 ml of 8 M NaOH (J.T. Baker), 1 g kaolin (Sigma-Aldrich) and 4 g of Na_2SO_4 (Sigma-Aldrich, ≥ 99.0%). NaCl (J.T. Baker, 99.5%) was incorporated by partly substituting the amount of sulphate. The concentration for NaCl was relative to the amount of sulphate using mol-%. The solution was stirred at room temperature and poured into 50 ml Teflon coated steel autoclave. The synthesis was completed in VWR VENTI-Line Prime drying oven at 200 °C with a heating rate of 5 °C/min. After 48 h crystallisation time, the oven was allowed to freely cool down to room temperature. The product was washed with 40 ml of distilled water using Heraeus Biofuge Stratos centrifuge operating at 3000 rpm for 5 min per cycle. The washing cycle was repeated four times to obtain a pure product. The product was dried until dry or overnight at 80 °C. The sample was then ground in an agate mortar and heated in a reducing Formier 10 (10% H_2 + 90% N_2) atmosphere in Elite TSH12/70/300-2416CG furnace at 700 °C for 2 h using a heating rate of 3 °C/min. After the heating the sample was ground again. Using these synthesis steps, a batch of samples labelled as Na-CAN (sodium cancrinite) with Cl was prepared. The initial point of starting was to introduce different anions into the structure. Therefore, replacing NaCl with other sodium halides as starting materials was tested first. Next, also Li, K, and Ca halides were investigated. The syntheses for the other salt substitutions (**Table 2**) were done using the same steps.

Table 2. Salts used in cancrinite syntheses with their manufacturer information.

Salt	Manufacturer	Purity (%)
NaBr	Fluka	≥ 99
NaF	Merck	-
NaI	E. Merck	-
KCl	EMSURE	-
KBr	Fluka Analytical	-
KI	Merck	-
LiCl	Acros	99
LiBr	Merck	-
LiF	Aldrich-Chemie	-
LiI	Sigma-Aldrich	99
$CaCl_2 \cdot 6\ H_2O$	Riedel-De Haën	-
CaI_2	Alfa Aesar	99.5

2.2 Characterisation Methods

2.2.1 Powder X-ray diffraction (PXRD)

The phases and the purity of the samples were confirmed using PANalytical Aeris diffractometer with PIXcellD-Medipix detector and copper Kα radiation ($K_{\alpha 1}$ = 1.5406 Å and $K_{\alpha 2}$ = 1.5444 Å) operating at 40 kV and 7.5 mA. The instrument was equipped with a divergence slit of 1/4° with a step size of 0.0217°, Ni beta-filter, 0.04 rad Soller slits, 13 mm mask, 9 mm anti-scatter slit, and beam knife set to high position.

The quantitative phase identification and analyses were done using PANalytical HighScore Plus software by comparing the measured experimental patterns to the reference patterns found on the ICDD PDF4+ database.

2.2.2 X-ray fluorescence (XRF)

The elemental composition of the samples was investigated using PANalytical Epsilon 1 spectrometer with internal Omnian calibration and an Ag-anode X-ray tube. The XRF measurements were done using “Na 1h” program, which conducted four measurement cycles with different parameters in each that are presented in **Table 3**. More information in **Table S1-**

S4. The XRF results have been recalculated according to the ions of interest and the most common impurities.

Table 3. The parameters of each measurement cycle done in the "Na 1h" program.

Measurement	Filter	Detector mode	Acceleration voltage (kV)	Measurement time (s)	Measurement range (eV)
1	Ag	Normal	50	120	2-34
2	Cu	Normal	50	300	2-34
3	Al	High	12	180	Automatic
4	-	High	10	3000	0.9-4.0

2.2.3 Diffuse reflectance spectroscopy

The colour of the samples and its change were investigated after UV irradiation using diffuse reflectance spectroscopy. The measurements were performed using integrating sphere, in which the lamp used to illuminate the measurement was Avantes AvaLight-DHc using the halogen light source. The white reference for the measurements was MgO to compare the colour of the synthesised sample prior to UV irradiation. The samples were excited with 254 nm using a UVP model UVLS-24 UV EL, 4 W 254/365 nm handheld lamp for 5 min, after which the reflectance was measured instantly. The spectra were collected using Avantes Avaspec HS-TEC CCD spectrometer with 1000 µm VIS/NIR 0.037NA PC04 optical fibres or Agilent Cary 60 UV-Vis Spectrophotometer with $BaSO_4$ as the white reference. When Cary 60 was used, it is specifically specified in the discussion. Otherwise, the measurements were done with HS-TEC spectrometer. Additionally, some measurements were done with 302 nm using a UVP model UVM-57, 6 W lamp and 365 nm using a UVP model UVLS-24 UV EL, 4 W 254/365 nm handheld lamp.

2.2.4 Thermotenebrescence

Thermotenebrescence was measured using Avantes FCR-7UVIR400-2-6X350-HTX optical fibre and Avaspec HS-TEC CCD spectrometer. The reflectance was measured before heating or irradiating the sample with the same UV lamp, as mentioned in 2.2.3, and the sample was used as the white reference. The thermotenebrescence measurement consists of three measurements, two of which are for the correction of the reflectance signal: (1) measuring reflectance of noncoloured, heated a sample; (2) measuring reflectance of coloured and heated samples; and (3) colouring sample and letting it spontaneously fade without heating. The

noncoloured sample was heated to 400 °C at a rate of 3 °C/s using MikroLab Thermoluminescent Materials Laboratory Reader RA ’04 followed by a reflectance measurement using the data collection time of 1 s (500 ms integration time, 2 averages). This way a reflectance spectrum was measured every second during the heating. A fresh sample was irradiated for 5 min with a 254 nm UV lamp followed by repetition of the same heating and measuring steps as for the “noncoloured, heated” sample. Lastly, a fresh sample was irradiated for 5 min under 254 nm UV lamp, after which the spontaneous fading was measured for 10 min under incandescent light.

2.2.5 Photochromism excitation spectra

The photochromism excitation spectra were measured by irradiating the sample with 400-200 nm for 10 min using SB522 150 W Xe-arc lamp combined with a LOT MSH 300 monochromator. The measurements were performed every 20 nm. For each measurement, a fresh sample was used, and it was set as the white reference prior to irradiation. The spectra were measured by illuminating the sample with Ocean Insight halogen light source HL-2000-LL using the same HS-TEC spectrometer and optical fibre as mentioned in 2.2.3. The colour intensity was obtained by integrating the reflectance minima.

2.2.6 Rise and fade of photochromism colouration

By continuously irradiating the sample and recording the rise of photochromism colouration, the colour intensity could be calculated by integrating the reflectance spectra. The sample was excited with the same 254 nm UV lamp as previously mentioned in 2.2.3 while performing a continuous reflectance measurement from 180 to 1120 nm with the same HS-TEC spectrometer as in 2.2.3 and FC-UV600-1-SR optic fibre under Ocean Insight halogen light source HL-2000-LL. The data was collected every second for 2 h.

The fade curve of photochromism was measured by saturating the sample by irradiating it with 254 nm UV lamp mentioned in 2.2.3 for 60 min to fully saturate the sample and then bleaching it under the Ocean Insight halogen lamp for 70 min. The reflectance was measured using the same data collection parameters as for the rise curve in 2.2.6.

2.2.7 Photoluminescence (PL)

The PL properties of the samples were investigated using Varian Cary Eclipse Fluorescence Spectrophotometer equipped with a 150 W xenon lamp and Hamamatsu R928 photomultiplier

tube. The parameters for the PL measurements in phosphorescence mode are the following: gate time of 5.0 ms, delay time of 0.1 ms, excitation slit width of 10 nm, emission slit width of 5 nm, and a step size of 0.2 nm with the detector voltage of 800 V. With 302 and 365 nm excitation, emission width slit of 10 nm was used. The excitation harmonic wavelength can be seen (e.g. for $\lambda_{ex.}$ = 254 nm, the multiple would be ~508 nm and ~604 nm for $\lambda_{ex.}$ = 302 nm).

2.2.8 Additional characterisation methods

Field-emission Scanning Electron Microscopy (FE-SEM) and energy dispersive X-ray spectroscopy (EDS) measurements were done using Thermo Scientific Apreo S microscope and Oxford Instruments UltimMax 100 EDS. The samples were prepared for analysis by dropping a few milligrams of particles onto thin moulds of SpeciFix-40 (Struers) or Petropoxy 154 (Burnham Petrographics) epoxies and curing the mixture. The particle-containing epoxy sheets were milled with broad Ar ion beam mill (ArBlade 5000, Hitachi High-Technologies) at an accelerating voltage of 5 kV revealing flat cross-sections of the embedded particles. Before SEM-EDS analysis, the exposed surface was coated with ~2 nm of Pt using a sputter coater (Q150V ES+, Quorum Technologies). Electron imaging and X-ray data collection and analysis were done using AZtec v6.1 software (Oxford Instruments). Acceleration voltages of 7 and 15 kV were used for the imaging and compositional analysis. These SEM-EDS analyses were performed by Ermei Mäkilä from Department of Physics and Astronomy, University of Turku.

The thermoluminescence (TL) glow curves of the samples were done by heating the sample to 500 °C at a heating rate 10 °C/s using the MikroLab Thermoluminescent Materials Laboratory Reader RA '04. Prior to irradiation, possible electron traps were bleached by heating the sample to 500 °C. The samples were measured after UV irradiation using 254 nm for 5 min and X-ray irradiation for 26 min (**Table 4**) using PANalytical Epsilon 1 as the source of X-rays. The measurement was carried out after a minute wait following the irradiation. Blackbody radiation of the measurement setup is visible after 400 °C in the glow curves.

The optically stimulated luminescence (OSL) properties were investigated by irradiating a sample with X-rays using PANalytical Epsilon 1 and stimulating it with 980 nm laser using Roithner LaserTechnik RLTMFC-980-50W-1 laser. A film was cast for OSL measurements by mixing the sample with an organic polymer. The sample, 2-butanone, ethanol, and Triton X-100 were mixed in a Philips Minimill PW4018/00 ball mill for 10 min at speed 1. Polyvinyl butyral and benzyl butyl phthalate were added and remixed for 2 min at speed 5. The suspension was then transferred on 0.1 mm thick Xerox Premium Transparencies and casting it into 350 µm thick coating using Erichsen Coatmaster 510 with doctor blade. The film was

also used for X-ray imaging by exciting the sample for 26 min with X-rays (**Table 4**. The parameters of each measurement cycle done in the "Academia 20 min" program.**Table 4**) using PANalytical Epsilon 1 and running it through VistaScan Mini Easy.

Table 4. The parameters of each measurement cycle done in the "Academia 20 min" program.

Measurement	Filter	Detector mode	Acceleration voltage (kV)	Measurement time (s)	Measurement range (eV)
1	Ag	Normal	50	300	2-34
2	Cu	Normal	50	600	2-34
3	Al	High	12	300	Automatic
4	-	High	10	600	Automatic

3 Results and Discussion

3.1 Background on the samples

During this project, samples with different ions with varying concentrations were synthesised. The samples were characterised and tested and measured for their photochromic and luminescence properties. The samples were characterised by PXRD, XRF, and the PL and colour change properties were measured. The PXRD results of the intermediate products, before reducing, are also shown so the effect of reductive heat treatment can be seen. The initial point of starting the substitutions was preparing a series with differing amounts of NaCl, which then was a point of reference for other halide salt substitutions. It should be kept in mind that the XRF results as a whole may be inaccurate due to the device's difficulties in detecting especially the sodium concentration accurately.

The acquired samples formed columnar and needle-shaped crystals which broke during the washing cycles. The powder, after drying and grinding, was white and polycrystalline. Buhl et al.[1] reported that the transition into nosean happened at 930 °C in a cancrinite sample synthesised using kaolin. Although their thermoanalyser results showed that cancrinite phase was still pure at 850 °C with a holding time of 30 min, to ensure the phase remained cancrinite, a lower temperature of 700 °C for 2 h was chosen. They also reported that the maximum framework expansion happened at 710 °C.

After reducing at 700 °C, the samples were varying shades of grey, white, pale yellow, and pale pink. Later in some samples, this colour changed to darker grey. A temperature trial was done for a few samples which also concluded the 700 °C being the suitable temperature for reduction but those tests are not reported in this thesis.

The formula used in the following sections for the synthesised cancrinite samples $(Na,M)_8Al_6Si_6O_{24}(X_{y\%},S_{z\%})_2$, where M is any cation used and X is any anion used, is nominal based on precursors' molar ratios. The solubility and the synthesis environment affect the M:Na and X:S ratios in the actual synthesis product. In the formula, y indicates the amount (in mol-%) of halides added compared with the amount of sulphur in the protocol of Buhl J. et al. 2019, while z indicates the amount of sulphur used in the reaction compared with that of the protocol of Buhl J. et al. 2019. That is, both y and z are calculated with respect to 4 g of Na_2SO_4. The sum of y and z may exceed 100 % indicating that an excess of extra-framework anions were present in the reaction mixture.

3.2 Na-CAN

The results of the measured X-ray diffraction of all samples are presented in **Figure 3**. The diffractograms of samples show the characteristic reflections of cancrinite phase (04-012-0446)[43] at 2θ ≈ 13.9°, 18.3°, 24.3°, and 27.5°, except for sample containing NaCl with the concentration of 50%. The major phase in this sample is sodalite (08-008-4863)[43], while still having the most intense reflection of cancrinite present. According to these results, it can be determined that the synthesis for ion substitution was successful leading to desired material. The XRF results also support the formation of the right phase (**Table S1**), although having large amount of iron and titanium impurities characteristic for kaolin, as well as some traces of manganese. The amount of substitution ions ending up in the structure of the material cannot be said for sure from XRF results due to the unreliability but can be used as an estimate.

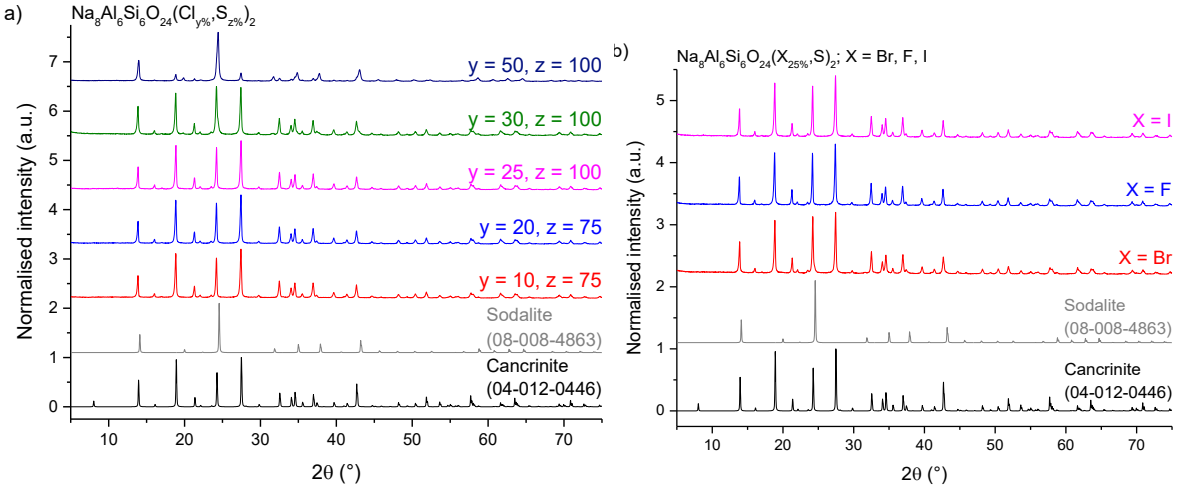

Figure 3. PXRD diffractograms of Na-CAN samples a) with varying NaCl concentration and c) with 25% concentration of other sodium salts before reducing compared to reference patterns of cancrinite (04-012-0446)[43] and sodalite (08-008-4863)[43].

After reducing, the samples were ivory to greyish-white coloured. The samples were characterised again using PXRD and XRF (**Figure 4**). It can be seen from the diffractograms that the phase successfully transformed into hydroxycancrinite (01-078-2494)[43] due to the reductive heat treatment. According to Buhl et al.[1], the reflection at 9.7° and a slight left shoulder on the reflection at 24.3° would indicate the presence of nosean. On these Na-CAN samples the 9.7° reflection is not visible, but a slight left shoulder has started to form on some samples, like $Na_8Al_6Si_6O_{24}(Cl_{10\%},S_{75\%})_2$. The reflections indicating nosean are minor in the Na-CANs, which means the reduction temperature and time was suitable. Most samples had a reflection at 17.1° which remained unidentified due to its very low intensity. The same iron and titanium impurities persist also in the reduced samples. The effect of substitution can also be

seen in the unit cell parameters (**Table 5**). Surprisingly, the largest unit cell can be found in $Na_8Al_6Si_6O_{24}(Cl_{25\%},S_{100\%})_2$ sample, opposed to what was predicted in literature. This could be due to more Cl^- ions being similar size to S^{2-} and more Cl^- ions were present in the structure. The enlargement of the unit cell of $Na_8Al_6Si_6O_{24}(I_{25\%},S_{100\%})_2$ can also be seen, which indicates that at least some I^- ions are in the structure. The unit cell parameters of $Na_8Al_6Si_6O_{24}(Cl_{10\%},S_{75\%})_2$ indicates the expansion of the c-axis. This can be seen in other samples as well, which suggests that the substitution ions replace some of the S^{2-}, OH^- ions or possible H_2O molecules.

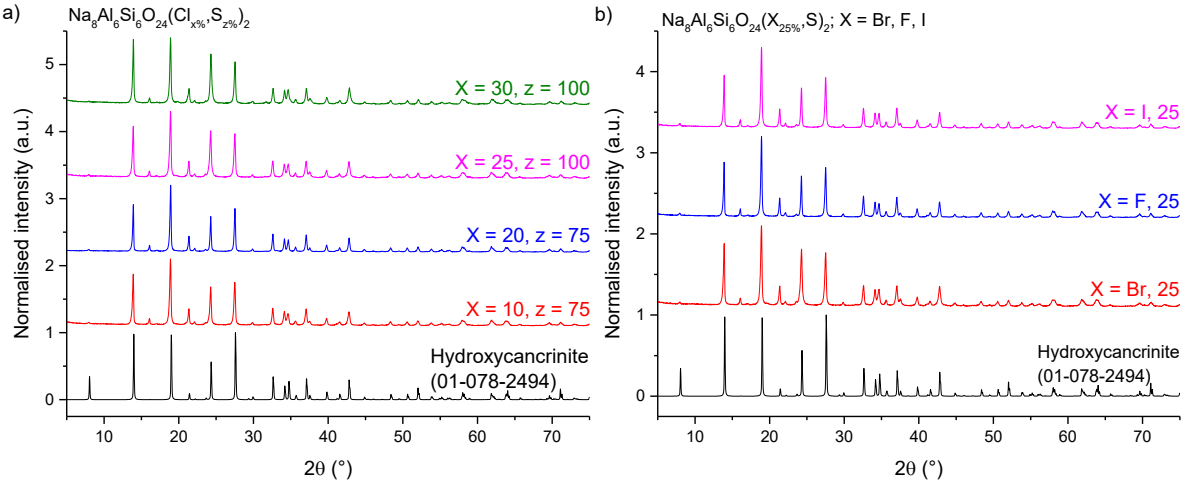

Figure 4. PXRD patterns of the reduced Na-CAN samples containing a) chloride or b) other anions compared to the reference pattern of hydroxycancrinite (01-078-2494)[43].

Table 5. Unit cell parameters and volume of Na-CAN samples.

Sample	a (Å)	c (Å)	Unit cell volume (Å)
$Na_8Al_6Si_6O_{24}(Cl_{10\%},S_{75\%})_2$	12.64355	5.16678	715.30
$Na_8Al_6Si_6O_{24}(Cl_{20\%},S_{75\%})_2$	12.64599	5.16114	714.80
$Na_8Al_6Si_6O_{24}(Cl_{25\%},S_{100\%})_2$	12.68778	5.18006	722.17
$Na_8Al_6Si_6O_{24}(Cl_{30\%},S_{100\%})_2$	12.64778	5.16129	715.02
$Na_8Al_6Si_6O_{24}(Br_{25\%},S_{100\%})_2$	12.64878	5.16508	715.66
$Na_8Al_6Si_6O_{24}(F_{25\%},S_{100\%})_2$	12.65100	5.15890	715.05
$Na_8Al_6Si_6O_{24}(I_{25\%},S_{100\%})_2$	12.65180	5.16060	715.38

Reflectance was measured after the phase confirmations. It can be said from the difference spectra of the reflectances (

Figure 5a) that the photochromism was successfully brought out, and a clear regression happens in the colour change property in the NaCl series with the increase of Cl concentration.

The samples with different sodium halides, with the concentration of 25%, show properties of photochromism in their spectra (

Figure 5b), but depth of the minima is weaker compared to the samples with NaCl. The colour change was not easily detectable by eye and was only seen faintly in samples $Na_8Al_6Si_6O_{24}(\mathbf{Cl_{10\%}},S_{75\%})_2$ and $Na_8Al_6Si_6O_{24}(\mathbf{Cl_{20\%}},S_{75\%})_2$. The depth of the minimum is 7% and position is at 633 nm for $Na_8Al_6Si_6O_{24}(Cl_{10\%},S_{75\%})_2$. It is reasonable to think that the excess amount of sulphur would easily create sulphur-rich material, hence the initial colour and absorption in the UV spectrum.

For photochromic sodalites, it was predicted that larger anions would cause the absorption wavelength to shift to higher wavelengths. In the Na-CAN sample, the opposite can be seen. The structure of photochromic sodalites and cancrinite differ, which affects the absorption properties. It could also be that the possibly differing location of the anion causes the material to vary from literature. Since S^{2-} and Cl^-/Br^- (1.81 Å/1.96 Å)[44] are close in size, the properties behave more similarly and predictably, while the I^- ions (2.2 Å)[44] are much bigger and F^- ions (1.33 Å)[44] are much smaller. This could cause the smaller ion to substitute better or not at all. The photochromic properties of chloride variants are superior which would indicate better substitution, and more vacancies and radicals with ions similar in size. The higher substitution can be seen in Na-CAN XRF results which possibly lead to the enhancement of photochromic property of $Na_8Al_6Si_6O_{24}(Br_{25\%},S_{100\%})_2$ sample.

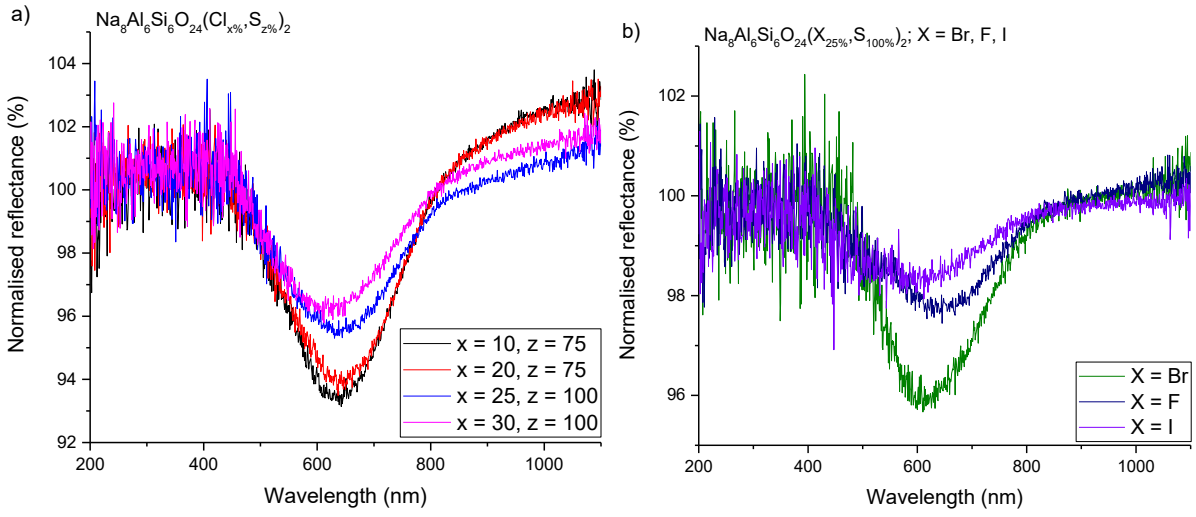

Figure 5. The reflectance spectra of Na-CAN samples substituted a) with 10-30% concentration of sodium chloride and b) with 25% concentration of sodium salts of bromide, fluoride and iodide.

The colour of the best sample, $Na_8Al_6Si_6O_{24}(Cl_{10\%},S_{75\%})_2$, was photographed using Canon EOS 250D camera after irradiating a part of its surface for 5 min with 254 nm (**Figure 6**). Due to the colour being faint, but still noticeable, further experiments were conducted on this sample.

Figure 6. Right side of $Na_8Al_6Si_6O_{24}(Cl_{10\%},S_{75\%})_2$ sample irradiated with 254 nm for 5 min, left side covered during irradiation. The photo has been enhanced to properly display the colour change.

The excitation spectrum, and fade and rise curves of the photochromic colour were measured to get information on the behaviour of the photochromism on the sample. This way the best wavelength and time for excitation are found and more information on the fading time is gained. For the lamp used to excite the photochromism to get the excitation spectrum, the UV range intensity is weaker than Vis range intensity. To take this into account, correction factors were used for the data.

According to the excitation spectrum (**Figure 7a**), the best wavelengths for irradiation are 240 and 300 nm. To confirm this, new reflectance measurements were taken using 254, 302, and 365 nm with the irradiation time of 5 min (**Figure 7b**). The colour change was the best with 254 and 302 nm, but also irradiation with 365 nm produced photochromic response. The time needed to fully saturate the sample is 9 min, which can be seen in **Figure 8a**. The fade curve (**Figure 8b**) shows that fully saturated sample fades back to its original colour within 70 min under incandescent light. The quick colouration and spontaneous fading of colour are similar to photochromic sodalites which also fade rather quickly e.g. hackmanite.

These results strengthen the theory that the mechanism works similarly to hackmanite, since hackmanite is known for its fast colouring and bleaching rates. The position of the minima of the Na-CAN samples is also alike to hackmanite samples, but the absorption band in UV spectrum is different. In hackmanites, a narrow absorption band can be seen at 248-295 nm and 310-320 nm[45], but in the tested sample, $Na_8Al_6Si_6O_{24}(Cl_{10\%},S_{75\%})_2$, the absorption band is wider

and is continuous from 200 to 400 nm (**Figure S1**). For hackmanites, the suggested mechanism is $S^{2-} \rightarrow S^{-} + e^{-}/S_2^{2-} + e^{-}$, which corresponds to UV absorption in S-containing ions by Song et al.[45]

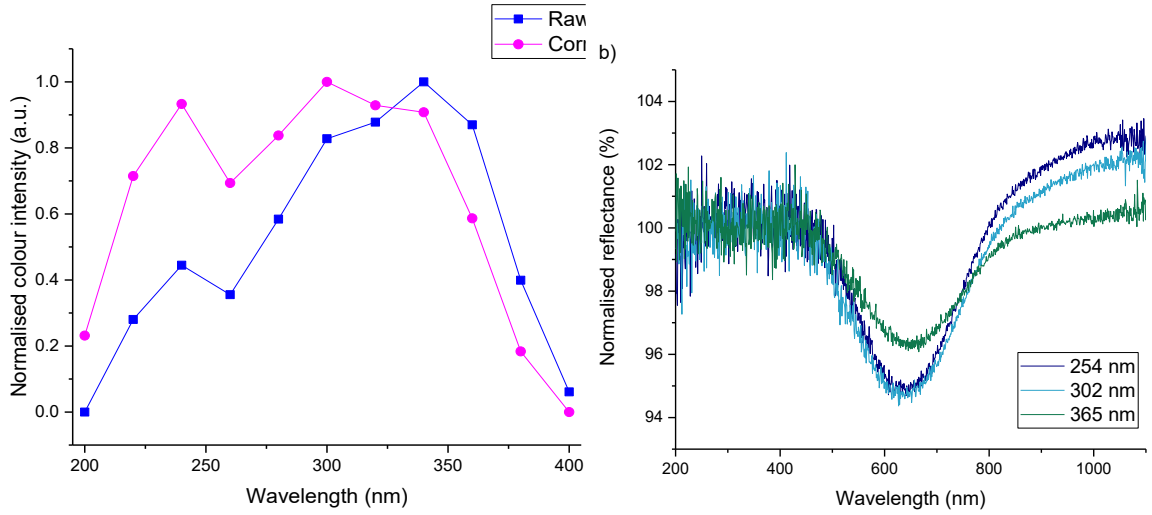

Figure 7. a) Photochromism excitation spectrum of $Na_8Al_6Si_6O_{24}(Cl_{10\%},S_{75\%})_2$ sample. b) The same sample irradiated with 254, 302, and 365 nm.

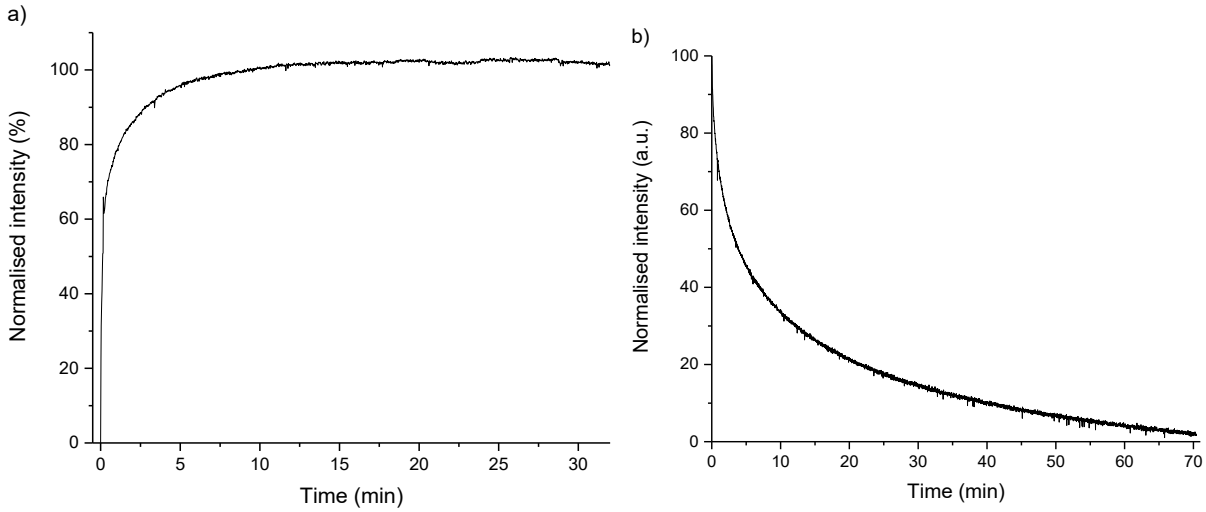

Figure 8. a) Photochromism rise curve and b) fade curve of $Na_8Al_6Si_6O_{24}(Cl_{10\%},S_{75\%})_2$ sample.

From the TT curve, the needed energy to bleach the sample can be calculated (**Figure 9**). Although, some random scattering can be seen on the spectrum, the calculated energy to bleach is 0.29 eV for $Na_8Al_6Si_6O_{24}(Cl_{10\%},S_{75\%})_2$ sample. This would mean that the electron traps formed in the material can be released relatively easy, which does align with its fast bleaching time under incandescent light.

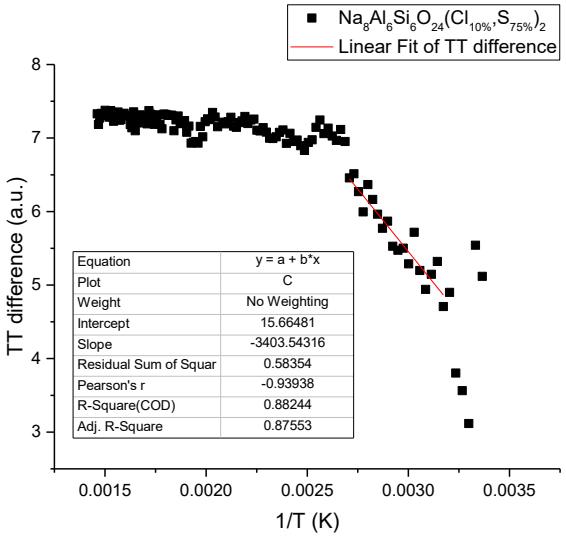

Figure 9. Initial rise analysis of the TT curve of $Na_8Al_6Si_6O_{24}(Cl_{10\%},S_{75\%})_2$ sample.

From the reflectance spectra, it can be concluded that the Na-CAN samples behave somewhat similarly to photochromic sodalites, but the properties are much weaker. The reflectance minimum does shift according to the anion, but not in the predicted way. Instead of the samples containing Br and I shifting to longer wavelengths[32,35], the samples with smaller anions have minimum at slightly longer wavelengths. It should also be noted that most samples had one or two reflectance minima before irradiation caused the samples absorbing specific wavelengths despite not having UV induced colour centres, as will be shown in **Figure 28**.

The PL properties of the Na-CAN samples were measured using 254, 302, and 365 nm excitation. The PL emission spectra (**Figure 10**) show some emission coming from the samples at wavelengths 425, 627, and 685 nm when using 254 nm to excite the samples and excitation with 302 nm produces broad peak from 414 to 790 nm. The emission peaks coming from the samples are very low in intensity, hence why the emission cannot be seen by eye. The samples produced no emission with 365 nm excitation.

Out of the Na-CAN samples, $Na_8Al_6Si_6O_{24}(Cl_{30\%},S_{100\%})_2$ and $Na_8Al_6Si_6O_{24}(Br_{25\%},S_{100\%})_2$ samples have the strongest emission compared to the other samples. This could be due to the anion sizes complementing each other, and the higher substitution concentration creating more defects. The impurities e.g. Ti, Mn^{2+}, Fe^{3+} can cause luminescence centres as well.

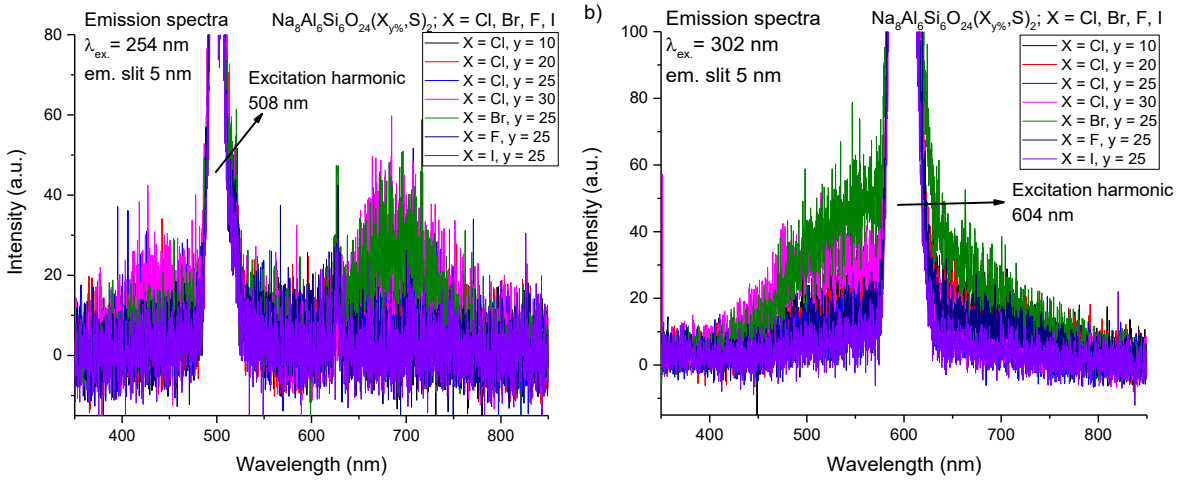

Figure 10. PL emission spectra of the Na-CAN samples using excitation wavelength of a) 254 nm with excitation harmonic of 508 nm visible and b) 302 nm with excitation harmonic of 604 nm visible.

3.3 Na,K-CAN

The PXRD patterns of the Na,K-CAN samples before and after reducing are presented in **Figure 11**. The patterns confirm that the samples were pure with minor impurity phases in the bromide variant indicated by the small reflections at 26.8° and 33.0°. These reflections, presumably, belong to sillimanite ($Al_2(SiO_4)O$) phase, which is likely to form due to the impurities of Ti and Fe in their oxide forms. The sodalite or the nosean phase reflections are not detected concluding the material formed correctly. The substitution can be seen as unit cell parameter and volume changes (**Table 6**) despite the diffractograms showing only minor shifts in the reflections. The biggest unit cell expansion can be seen in $(Na,K)_8Al_6Si_6O_{24}(I_{20\%},S_{100\%})_2$ sample due to the large anions. Notably, $(Na,K)_8Al_6Si_6O_{24}(Cl_{20\%},S_{100\%})_2$ sample has larger unit cell compared to its bromide counterpart. According to the unit cell parameters of $(Na,K)_8Al_6Si_6O_{24}(Br_{20\%},S_{100\%})_2$ sample, more bromide was able to incorporate into the structure instead of potassium. The XRF results also suggest this (**Table S2**). The XRF quantities acquired of other Na,K-samples show successful substitution of sodium.

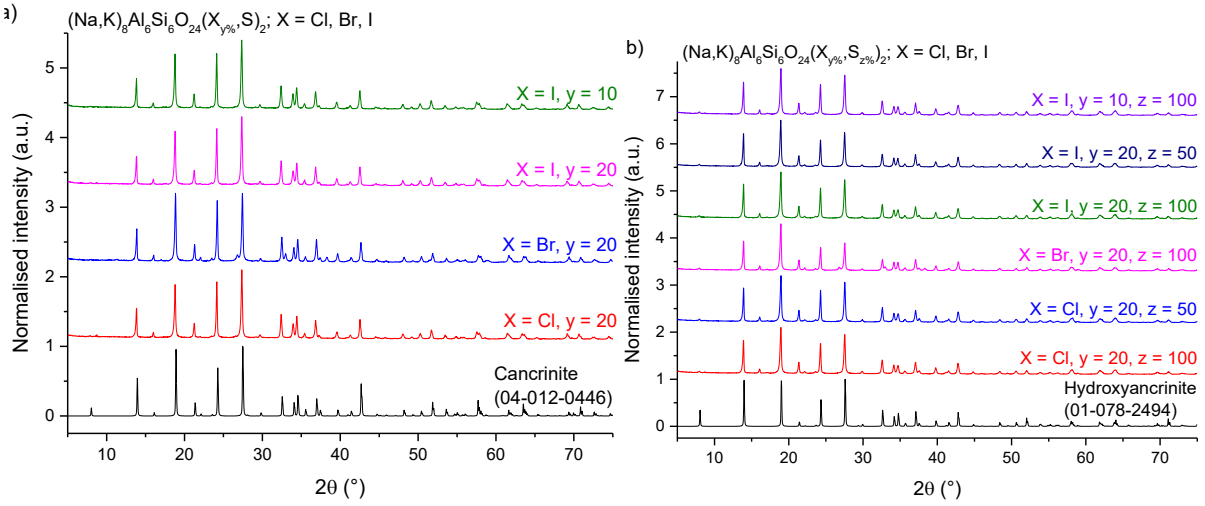

Figure 11. PXRD patterns of cancrinite samples with potassium salts a) before reducing compared to the reference cancrinite phase (04-012-0446)[43] and b) after reducing compared to the reference hydroxycancrinite phase (01-078-2494)[43].

Table 6. Unit cell parameters and volume of Na,K-samples.

Sample	a (Å)	c (Å)	Unit cell volume (Å)
$(Na,K)_8Al_6Si_6O_{24}(Cl_{20\%},S_{100\%})_2$	12.65587	5.15307	714.79
$(Na,K)_8Al_6Si_6O_{24}(Cl_{20\%},S_{50\%})_2$	12.65461	5.15245	714.57
$(Na,K)_8Al_6Si_6O_{24}(Br_{20\%},S_{100\%})_2$	12.64708	5.15654	714.28
$(Na,K)_8Al_6Si_6O_{24}(I_{20\%},S_{100\%})_2$	12.65687	5.15609	715.33
$(Na,K)_8Al_6Si_6O_{24}(I_{20\%},S_{50\%})_2$	12.65244	5.15758	715.03
$(Na,K)_8Al_6Si_6O_{24}(I_{10\%},S_{100\%})_2$	12.65571	5.15171	714.59

The reflectance spectra (**Figure 12**) show that cancrinite exhibits photochromism also with potassium halides. Compared to the sodium salts, the depth and the position of the minima have decreased and shifted to shorter wavelengths. The cause for this could be the slight increase in the parameter a. The broadening of the absorption band can be seen clearly in the $(Na,K)_8Al_6Si_6O_{24}(Br_{20\%},S_{100\%})_2$ sample. A major improvement in the depth can be seen in $(Na,K)_8Al_6Si_6O_{24}(\mathbf{I_{20\%}},S_{100\%})_2$ compared to $(Na,K)_8Al_6Si_6O_{24}(\mathbf{I_{10\%}},S_{100\%})_2$ sample. The improvement could be due to enough I^- ions found their way into the structure thus expanding the unit cell. This would lead to more vacancy sites therefore lowering the energy requirement to create colour centres, just like in photochromic sodalites presented in a paper by Colinet et al.[46] It also could be because photochromism and luminescence compete with one another with usually only one property dominating. In $(Na,K)_8Al_6Si_6O_{24}(\mathbf{I_{20\%}},S_{100\%})_2$ the dominating property is photochromism, while in $(Na,K)_8Al_6Si_6O_{24}(\mathbf{I_{10\%}},S_{100\%})_2$ it is luminescence. The

photochromic response weakened in the samples with halved amount of sulphide, $(Na,K)_8Al_6Si_6O_{24}(Cl_{20\%},S_{50\%})_2$ and $(Na,K)_8Al_6Si_6O_{24}(I_{20\%},S_{50\%})_2$, but created a sharp minimum at 355 and 378 nm, respectively.

The number of substituted ions in the structure and their sites are unknown, but the likelihood of substitution rate being higher than XRF lets us believe is highly possible due to used XRF spectrometer having difficulties detecting elements accurately. Nonetheless, some substitution ions ended up in the structure, since the position of the minimum and the broadness differs compared to Na-CAN samples. Out of all the Na,K-CAN samples, there were only two samples, $(Na,K)_8Al_6Si_6O_{24}(Cl_{20\%},S_{100\%})_2$ and $(Na,K)_8Al_6Si_6O_{24}(I_{20\%}, S_{100\%})_2$, with a clear but weak minimum at 542 and 566 nm, respectively. In these samples, the predicted shift to higher absorption wavelengths with larger anions can be seen clearly.

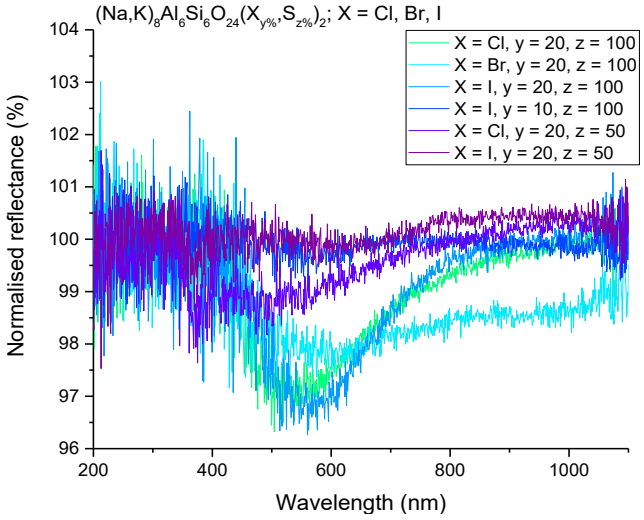

Figure 12. The reflectance spectra of the Na,K-samples when irradiated with 254 nm for 5 min.

The PL properties improved slightly with the addition of potassium salts compared to the sodium salt variants. In **Figure 13**, $(Na,K)_8Al_6Si_6O_{24}(I_{10\%},S)_2$ sample stands out with its blue emission at 430 nm. The emission corresponds to Ti^{4+} ions on a study done on alumina.[47] Though the studied material was different, it showed that titanium gives blue emission using electron-hole recombination energy, especially in the presence of Si atoms.[48] In other studies it is also shown that titanium is known to produce blue emission with the maximum being 410-440 nm[49,50]. For some reason, this sample allowed enough titanium to be incorporated into the structure causing enough luminescence centres to emit blue light. It should also be kept in mind that Fe is high as impurity, which could replace Al and Si in their tetrahedra, respectively. Slight peak formation can be seen from 650 to 900 nm which could indicate that Fe^{3+} has found a site. A possibility of Na replacement by Mn is also possible.[51,52] A small peak developing at 500 nm

would indicate that Mn^{2+} replaced some of the Na ions in the structure, but in these spectra, the excitation harmonic forms on top of it.

The emission is not strong in $(Na,K)_8Al_6Si_6O_{24}(I_{10\%},S_{100\%})_2$ and is formed in these particles without PeL. The lack of it could be explained by excess sulphur preventing PeL while not having enough potassium to cancel out this effect. The predominant impurity atoms, Ti and Fe, could also cause overlaps in the absorption bands or quenching, which could explain the weak properties of the samples.[53]

The line emission at 627 nm is characteristic for Eu^{3+} ion $^5D_0 \rightarrow {}^7F_3$ transitions[54,55] indicating the presence of Eu impurity ions. Another characteristic Eu^{3+} ion line emission at 707 nm with low intensity is caused by $^5D_0 \rightarrow {}^7F_4$ transition.[56] The possible presence of Eu atoms is also confirmed by XRF results showing Eu concentration being between 0 to 360 ppm in the Na,K-CAN samples. Though these are not the intended substitution ions, this strongly suggests that cancrinite readily accepts various of ions which can be also concluded from the small elevation around 500 nm.

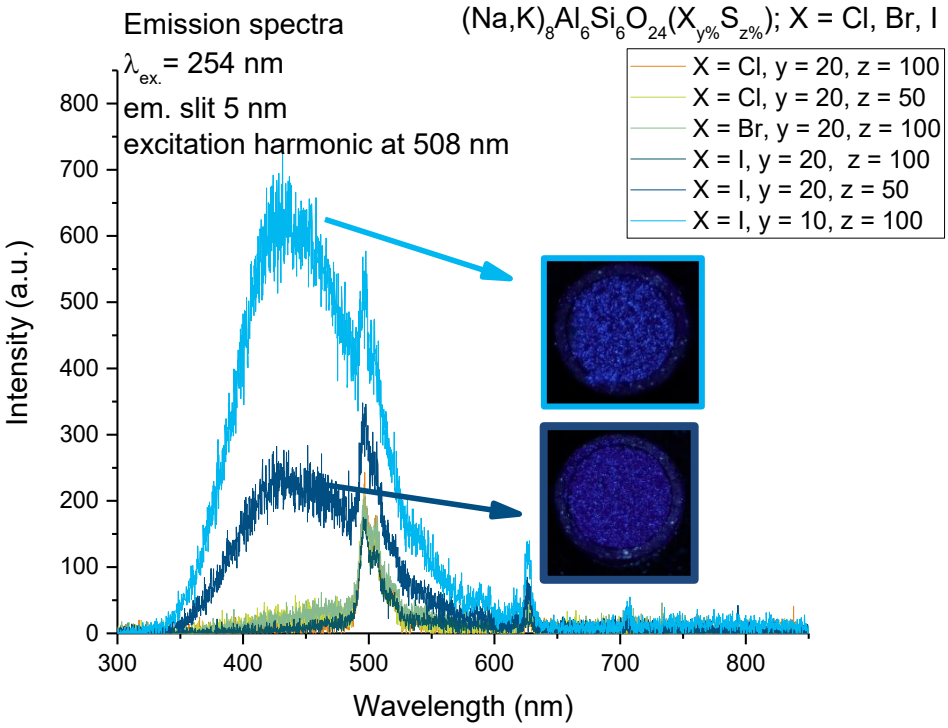

Figure 13. PL emission spectra of the Na,K-CAN samples excited with 254 nm with pictures of the two most intense samples. The excitation harmonic of 254 nm is the intense peak at 500 nm throughout the samples.

The secondary electron (SE) and backscattered electron (BSE) images (**Figure S2**) show that the sample mostly consist of small hexagonal cancrinite particles and some larger or longer particles caused by impurity phases. The cancrinite particles appear have roughly the

same elements, while the impurity phases seem to have more concentrated areas of similar or heavier atoms.

The SEM-EDS elemental mapping (**Figure 14**) of $(Na,K)_8Al_6Si_6O_{24}(I_{10\%},S_{100\%})_2$ reveals that the particles contain mostly aluminium, sodium, silicon, oxygen, potassium, and sulphur. This would indicate the phase in the sample is cancrinite with even distribution of potassium and sulphur, with the latter being the more dominant anion compared to iodide. According to XRF results, only miniscule amounts of iodide ended up in the sample replacing some S^{2-} ions. While the amount and location of I^- is still unknown, the effect of the KI salt addition can be seen in the optical properties.

A more concentrated area of Si, O, K, Ti, and Fe can be seen forming indicating to potassium silicate with iron and titanium (**Figure S4**). This is most likely due to the impurities found in kaolin forming some K, Ti, and Fe rich areas. While the Fe atoms are concentrated in the potassium silicate, Fe atoms can be found evenly distributed throughout the sample.

In this sample, the Na:K ratio is even, which caused by the sample being rich in sulphur. The even distribution of between the elements does not reveal, what is causing the luminescence. The luminescence could be also due to ions, not shown here, creating the luminescence centres. Some minor Mg thread impurities can be found (**Figure S3**). Although Mg impurities did not show on XRF results, it was expected that there are some Mg impurities in kaolin.

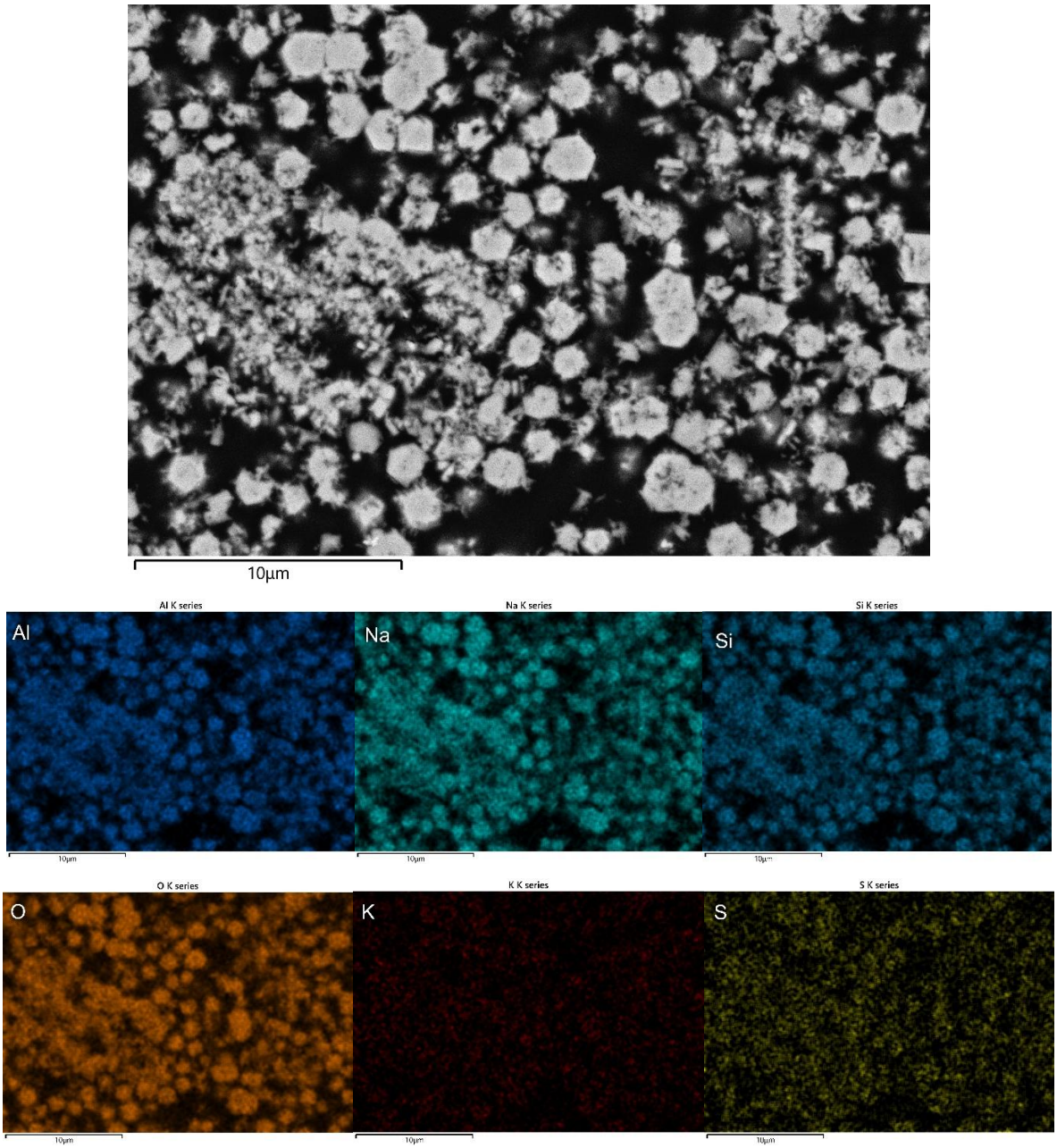

Figure 14. SEM-EDS elemental mapping with acceleration voltage of 7 kV of $(Na,K)_8Al_6Si_6O_{24}(I_{10\%},S_{100\%})_2$.

It can be concluded that in $(Na,K)_8Al_6Si_6O_{24}(I_{10\%},S_{100\%})_2$ sample, the cancrinite formed hexagonal particles correctly averaging in size of 2-3 µm. The cause for the luminescence centres, assumably, are the impurities found in kaolin. These results also strongly indicate that the Ti^{4+} ions are the cause for the blue particle emission.

3.4 Na,Li-CAN

The Na,Li-CAN samples show phase composition being cancrinite (04-012-0446)[43] before reduction (**Figure 15a**). The largest indicators of some other, impurity phase are the reflections

at 26.7°, 33.0°, and 38.3°. The impurity phase remains unidentified and persisted in the reduced samples as well (**Figure 15b**). The impurity reflections are not present in the samples containing LiI salt. This could be due to the size of iodide ions taking the whole site or due to the decreased degree of substitution forbidding the formation of other phases. A slight formation of a right shoulder of the 33.0° reflection in $(Na,Li)_8Al_6Si_6O_{24}(I_{5.5\%},\mathbf{S_{50\%}})_2$ sample can be seen, while $(Na,Li)_8Al_6Si_6O_{24}(I_{5.5\%},\mathbf{S_{100\%}})_2$ sample does not have it. This would indicate that sulphide ions are successfully saturating the structure prohibiting any other phases.

In other Na,Li-CAN samples, the ionic size difference between S^{2-} ions (1.84 Å)[44] and the substituted anion is much smaller compared to S^{2-} to I^- ions (2.2 Å)[44], excluding F^- ions (1.33 Å)[44], which are much smaller. The similar size can lead to higher degree of substitution or impurity phases, like in these samples. Although, the substitution cannot be seen well in the PXRD diffractograms, they can be seen in the unit cell parameter and the volume of it (**Table 7**). $(Na,Li)_8Al_6Si_6O_{24}(Cl_{20\%},S_{100\%})_2$ sample having the smallest unit cell volume and $(Na,Li)_8Al_6Si_6O_{24}(Br_{20\%},S_{100\%})_2$ sample having the biggest instead of samples with LiI salt. This indicates that the ions were successfully incorporated into the structure, but due to the smaller amount of substitution in $(Na,Li)_8Al_6Si_6O_{24}(I_{5.5\%},\mathbf{S_{100\%}})_2$ and $(Na,Li)_8Al_6Si_6O_{24}(I_{5.5\%},\mathbf{S_{50\%}})_2$, not enough I^- ions were present to fully enlarge the unit cells. In $(Na,Li)_8Al_6Si_6O_{24}(I_{5.5\%},S_{50\%})_2$ sample, the reduction of the S^{2-} ions caused the unit cell to shrink slightly. This possibly leads to better electron transfer which leads to improvement of the properties. The XRF data on these samples (**Table S3**) show the approximate composition of the sample due to lithium being too light to be detected with XRF. The amount of lithium can be roughly estimated by the amount of sodium in the sample, since the sodium concentration is roughly 13%. Also, notable amounts of Ti and Fe impurities are present.

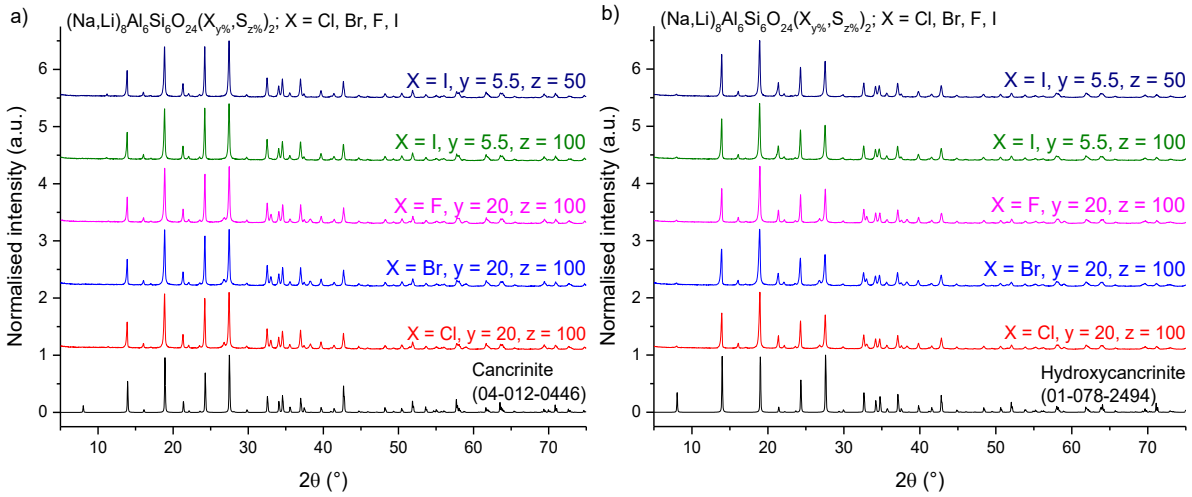

Figure 15. PXRD diffractograms of cancrinite samples containing lithium salts a) before reducing them compared to the reference cancrinite phase (04-012-0446)[43] and b) after reducing compared to the reference hydroxycancrinite phase (01-078-2494)[43].

Table 7. Unit cell parameters and volume of the Na,Li-CAN samples.

Sample	a (Å)	c (Å)	Unit cell volume (Å)
$(Na,Li)_8Al_6Si_6O_{24}(Cl_{20\%},S_{100\%})_2$	12.64591	5.15562	714.01
$(Na,Li)_8Al_6Si_6O_{24}(Br_{20\%},S_{100\%})_2$	12.65789	5.15814	715.73
$(Na,Li)_8Al_6Si_6O_{24}(F_{20\%},S_{100\%})_2$	12.64092	5.15324	713.13
$(Na,Li)_8Al_6Si_6O_{24}(I_{10\%},S_{100\%})_2$	12.64374	5.16274	714.76
$(Na,Li)_8Al_6Si_6O_{24}(I_{10\%},S_{50\%})_2$	12.64518	5.15750	714.63

It can be seen from the reflectance measurement results (**Figure 16a**) the samples have some photochromic response, but the depth of the minimum of the best sample, $(Na,Li)_8Al_6Si_6O_{24}(Cl_{20\%},S_{100\%})_2$, is less than 4%. To a degree, it can be said that these samples behave similarly to the Na,K-CAN samples. In both batches, the best photochromic response was acquired by substituting 20% of the S^{2-} ions with Cl^- ions without decreasing the amount of Na_2SO_4. In the Na,Li-CAN samples, it appears that I^- ion substitution could also lead to reasonable photochromic response, but due to scarce stock of the salt, only lower substitution concentration was tested. Notably, $(Na,Li)_8Al_6Si_6O_{24}(I_{5.5\%},\mathbf{S_{50\%}})_2$ sample has improved photochromic response compared to $(Na,Li)_8Al_6Si_6O_{24}(I_{5.5\%},\mathbf{S_{100\%}})_2$ sample. The reduction of the amount of sulphide did not affect the photochromic response positively in Na-/Na,K-CAN samples. In a study done by Norby et al.[57], they found the location of the Li^+ ions. The 6-membered rings host the tetrahedrally coordinated Li^+ ion to the surrounding four oxygen atoms. This would shrink the unit cell easing the electron transfer between the defects. In this

case, the less saturated structure caused more colour centres to form according to the results. However, the shrinkage of the unit cell would be unchanged by the larger anion to some extent.

The position of the minima is approximately the same across the Na,Li-CAN samples, but slight shift can be seen to the higher wavelengths with larger anions. In the Li-CAN samples, especially the samples containing LiI salt, the minimum at 380 nm is absorption possibly due to the sulphide-electron transfer[45]. This is particularly clear in $(Na,Li)_8Al_6Si_6O_{24}(I_{5.5\%},S_{50\%})_2$ when irradiated with 302 and 365 nm (**Figure 16b**). The potential explanation for this is that by not saturating the structure by S^{2-} ions, it creates more opportunities for defects and radicals to take place. It should also be noted that resolution is weak in the UV spectrum of the used spectrometer, which could make the results unreliable. To confirm changes in the UV spectrum, another set of spectra were recorded with Cary 60 UV-Vis spectrophotometer. The spectra of $(Na,Li)_8Al_6Si_6O_{24}(I_{5.5\%},S_{50\%})_2$ (**Figure 16c**) show that the absorption bands at 371 nm are a lot stronger compared to the spectra recorded with HS-TEC. Although, the absorption band does not decrease with irradiation, like it was theorised in literature, it does deepen with higher energy. This indicates that 254 nm creates the most amount of colour centres overall, but 302 nm compares in the UV spectrum absorption band, regardless HS-TEC showing otherwise. The same phenomenon can be seen in in $(Na,Li)_8Al_6Si_6O_{24}(I_{5.5\%},S_{100\%})_2$ sample which also has absorption bands at 380 nm with 302 and 365 nm irradiation. The absorption bands are slightly deeper. Most likely, due to increased amount of S^{2-} ions in the structure leading to more S-radicals.

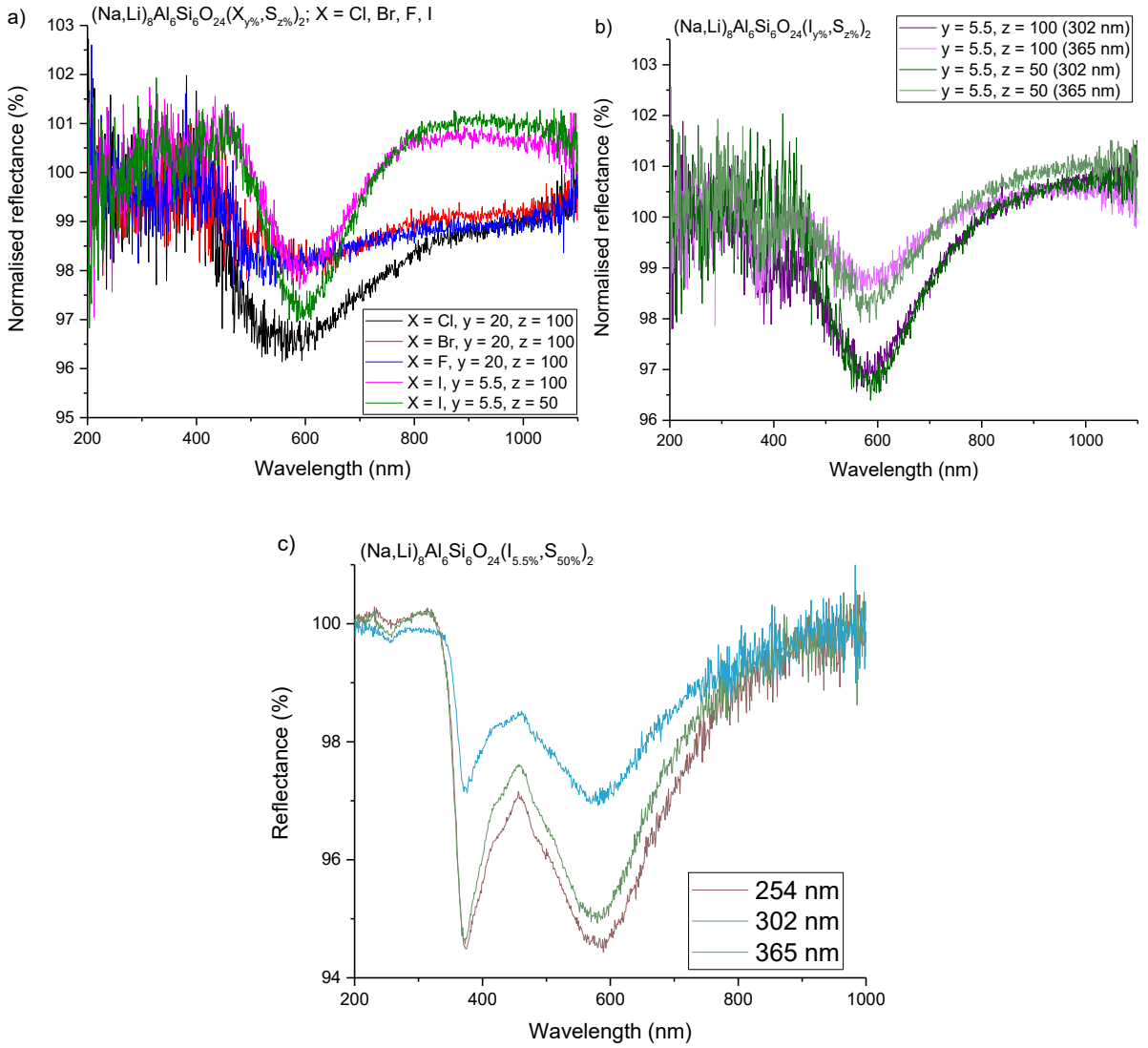

Figure 16. a) Reflectance spectra of the Na,Li-CAN samples irradiated by 254 nm for 5 min. b) Na,Li-CAN samples with 5.5% concentration of LiI salt irradiated with 302 and 365 nm for 5 min. The spectra for a) and b) were recorded with HS-TEC. c) Reflectance spectra of $(Na,Li)_8Al_6Si_6O_{24}(I_{5.5\%},S_{50\%})_2$ using Cary 60 spectrometer using 254, 302, and 365 nm.

The Na,Li-CAN samples had little to no emission, as can be seen in **Figure 17**. Some emission can be seen at 500 and 736 nm in $(Na,Li)_8Al_6Si_6O_{24}(Cl_{20\%},S)$ and $(Na,Li)_8Al_6Si_6O_{24}(F_{20\%},S)$, when the excitation wavelength was 254 nm. The similar emission spectrum shape can be seen in Na-CAN samples as well, while Na,K-CAN samples have more pronounced peak at ~500 nm. The reason for Na,K-CAN samples favouring the titanium impurity ions unknown, while Na- and Na,Li-CAN samples have emission evenly from the titanium and iron impurities. In the Na,Li-CAN samples, the size difference between the anions has a clear relation to the emission. The line emission at 627 nm can be found in all samples, which could indicate some Eu^{3+} impurities, similarly to Na,K-CAN samples.

The smaller cation and anions can allow more impurity ions to find their way into the structure. The weak emission could be caused because not enough luminescence centres are being created or some ion, e.g. iron, could be causing quenching. The emission is much weaker, when exciting the samples with 302 nm. The reminiscent shape to Na- and Na,K-CAN samples is still visible at 450 and 750 nm in most samples, but in $(Na,Li)_8Al_6Si_6O_{24}(I_{5.5\%},S_{50\%})$, the weak emission nearly covers the whole Vis-range. With 254 nm, this broad shape was not seen in this sample. The reason for this could potentially be titanium, iron, and manganese impurities combined with the lithium and sulphide ions in the structure. In literature, it has been reported that Fe^{3+} and Mn^{2+} have effects like these results.[53,58]

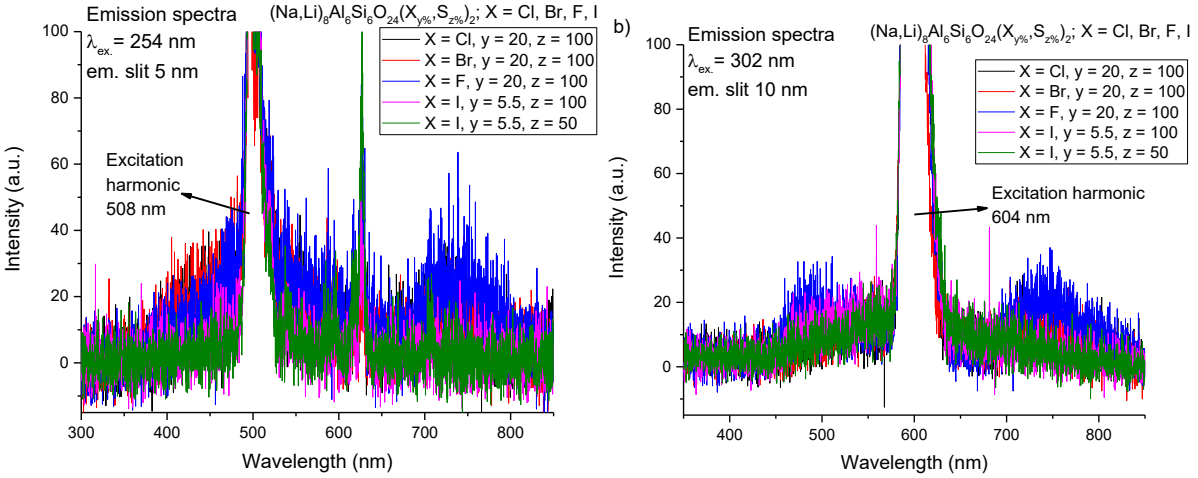

Figure 17. PL emission measurements of the Na,Li-CAN samples exciting with a) 254 nm with excitation harmonic of 508 nm visible and b) 302 nm with excitation harmonic of 604 nm visible.

3.5 Na,Ca-CAN

The Na,Ca-CAN samples were synthesised using the same steps as the previous samples, but after synthesising a sample with the addition of $CaCl_2$, the degree of substitution was lowered to prevent impurity phases. The divalent species would form other phases easier instead of incorporating into the structure due to the charge imbalance. The most likely phases in these samples were $Ca(OH)_2$, $HNaCa(SiO_4)$, and lawsonite ($CaAl_2Si_2O_7(OH)_2{\cdot}H_2O$), as can be seen in **Figure 18**, where the Na,Ca-CAN sample diffractograms are presented. The main phase in $(Na,Ca)_8Al_6Si_6O_{24}(Cl_{10\%},S_{100\%})_2$ before reducing is $HNaCa(SiO_4)$, but the main peaks of the cancrinite (04-012-0446)[43] phase are still visible. After reducing, the main phases for this sample are hydroxycancrinite (01-078-2494)[43] and lawsonite (04-012-1686)[43], but other phases can be also identified (**Figure 18c**). These additional phases are $CaO{\cdot}SiO_2$ (04-011-6361)[43] and $FeTiO_3$ (04-013-3472)[43]. Although, the reflections of these two phases get overshadowed by

the two main phases, the most prominent reflections cause some shoulders and larger reflections appear. The main phase in the Na,Ca-CAN samples with iodide and varying amounts of sulphate is hydroxycancrinite, although the peaks of lawsonite are still distinguishable.

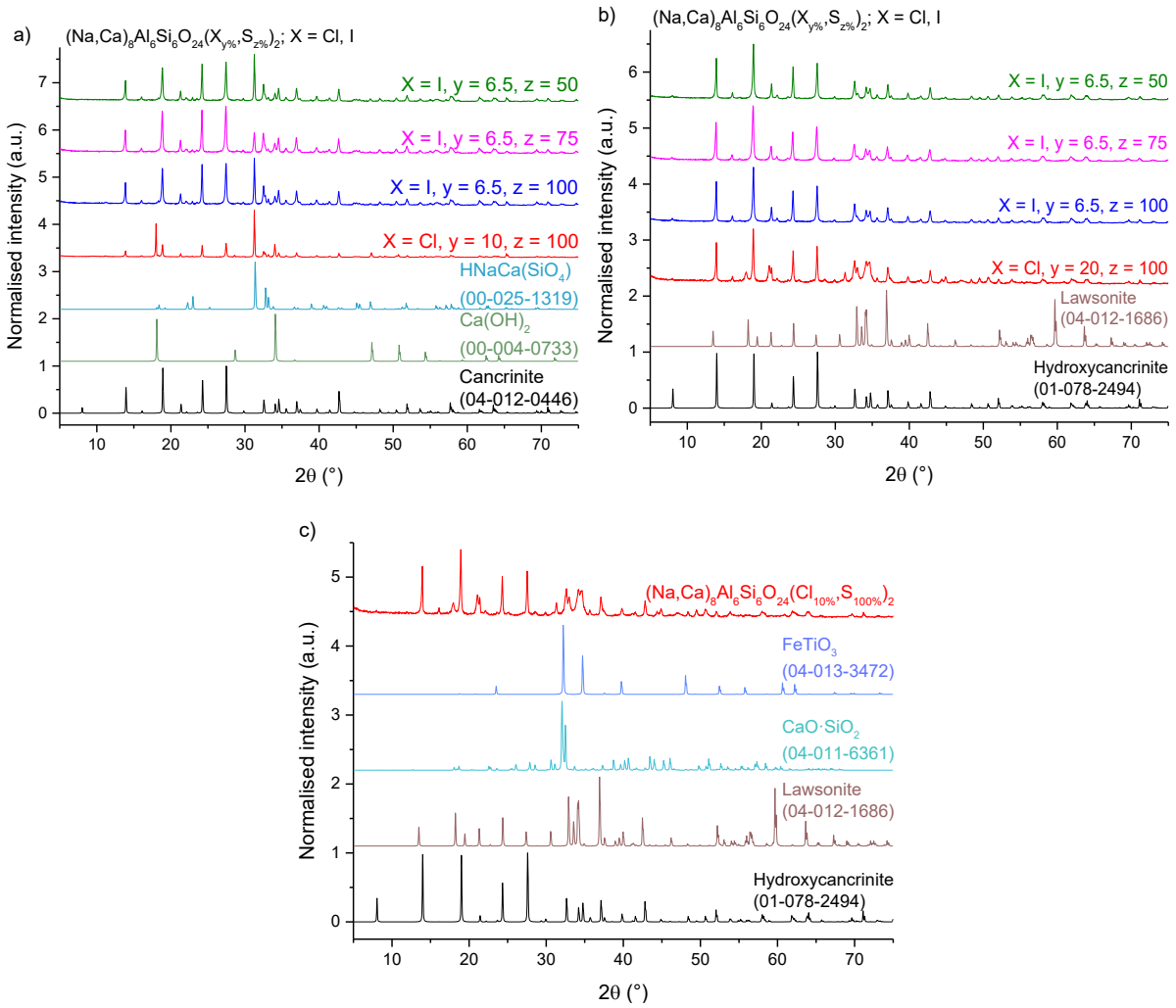

Figure 18. The measured PXRD diffractograms of the Na,Ca-CAN samples compared to the patterns found in data base a) before reducing and b) after reducing. c) More phases possibly found in $(Na,Ca)_8Al_6Si_6O_{24}(I_{10\%},S_{100\%})_2$.

Slight shifts of the reflections to lower angles can be seen in the diffractograms indicating partially successful incorporation of the bigger ions. The effect of the substitution can also be seen in the unit cell parameters (**Table 8**). The parameters suggest that more I^- ions are in the structure enlarging the unit cell, while the decrease in S^{2-} causes slight shrinkage of the unit cell along the c-axis. The shrinkage can be explained by the impurity phases leading to improper amounts of Na in the structure. This can also be seen in XRF results (**Table S4**)

Unexpectedly, the cell volume of $(Na,Ca)_8Al_6Si_6O_{24}(I_{6.5\%},S_{750\%})_2$ sample is the biggest. The reason for this sample being an outlier could be that the lesser amount of lawsonite phase. The increased amount of substitution ions could have a positive effect on the properties.

Table 8. Unit cell parameters and volume for Na,Ca-CAN samples.

Sample	a (Å)	c (Å)	Unit cell volume (Å)
$(Na,Ca)_8Al_6Si_6O_{24}(Cl_{10\%},S_{100\%})_2$	12.64878	5.15808	714.69
$(Na,Ca)_8Al_6Si_6O_{24}(I_{6.5\%},S_{100\%})_2$	12.63765	5.16262	714.06
$(Na,Ca)_8Al_6Si_6O_{24}(I_{6.5\%},S_{75\%})_2$	12.65560	5.16109	715.88
$(Na,Ca)_8Al_6Si_6O_{24}(I_{6.5\%},S_{50\%})_2$	12.64757	5.15868	714.63

To assess the photochromic properties of the Na,Ca-samples, reflectance was measured (**Figure 19a**). The samples that have the best photochromic response are $(Na,Ca)_8Al_6Si_6O_{24}(I_{6.5\%},\mathbf{S_{75\%}})_2$ and $(Na,Ca)_8Al_6Si_6O_{24}(I_{6.5\%},\mathbf{S_{50\%}})_2$ with the reflectance depth being 4%. The base colour of the samples was light grey which upon irradiation became darker grey (**Figure 19b**). Another noticeable difference is the width of the reflectance minima between the two samples. $(Na,Ca)_8Al_6Si_6O_{24}(I_{6.5\%},S_{75\%})_2$ sample appeared more grey after reduction which also made visualising the difference between before and after irradiation difficult. The cause for this grey colour is most likely the iron impurities found in kaolin.[59] This is intensified in reducing atmosphere.

There also seems to be a trend with the depth of the reflectance and the amount of sulphate. The samples with CaI_2 and varying amounts of sulphide successfully shifted to longer wavelengths, like predicted in literature. This shift indicates that more Ca^{2+} and I^- ions were able to be incorporated into the structure, even though being bigger than Na^+ and Cl^- ions, respectively. The deepening of the reflectance minima in the samples indicates that more defects are allowed in the structure, when it is not saturated with S^{2-} ions. This could mean that the excess S^{2-} ions do not allow enough defects to take place which forbids the formation of colour centres.

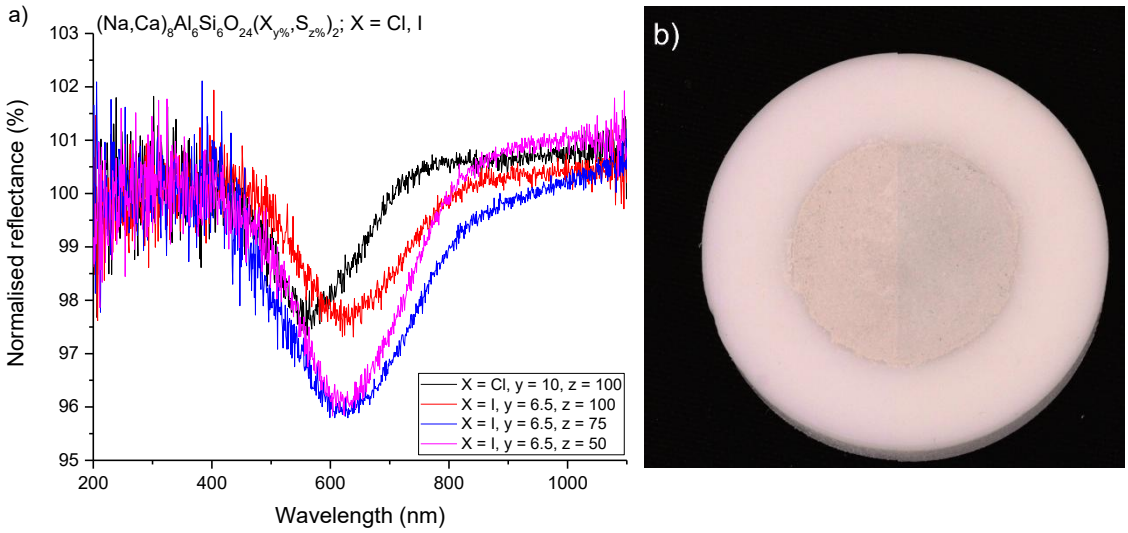

Figure 19. a) Na,Ca-CAN reflectance spectra measured using 254 nm irradiation for 5 min and b) right side of $(Na,Ca)_8Al_6Si_6O_{24}(I_{6.5\%},S_{50\%})_2$ sample irradiated with 254 nm for 5 min. The photo has been enhanced to present the difference more clearly.

Similarly to $Na_8Al_6Si_6O_{24}(Cl_{10\%},S_{100\%})_2$, more measurements were conducted on the $(Na,Ca)_2Al_6Si_6O_{24}(I_{6.5\%},S_{50\%})_2$ sample to give more information on the photochromic properties. The excitation spectrum (**Figure 20a**) indicates that 240 nm would be the best wavelength to irradiate the sample and secondary best would be 260 nm. It would also seem that irradiating with 300 nm, a photochromic response can be acquired, but only half as strong compared to 240 nm. To confirm this, new reflectance measurements were taken with 254, 302, and 365 nm. This time using irradiation time of 10 min, since the rise curve (**Figure 21a**) suggests that to obtain close to 80% saturation of the sample. This way it can be confirmed if better photochromic properties can be obtained with longer excitation time. To fully saturate the sample, irradiation time of 30 min would be needed.

The longer irradiation time intensified (**Figure 20b**) the photochromic response indicating higher trap concentration but could also indicate notable nonradiative recombination in $(Na,Ca)_2Al_6Si_6O_{24}(I_{6.5\%},S_{50\%})_2$ sample. Although the change was subtle from 4 to 5%, it made the visualisation of the colour clearer.

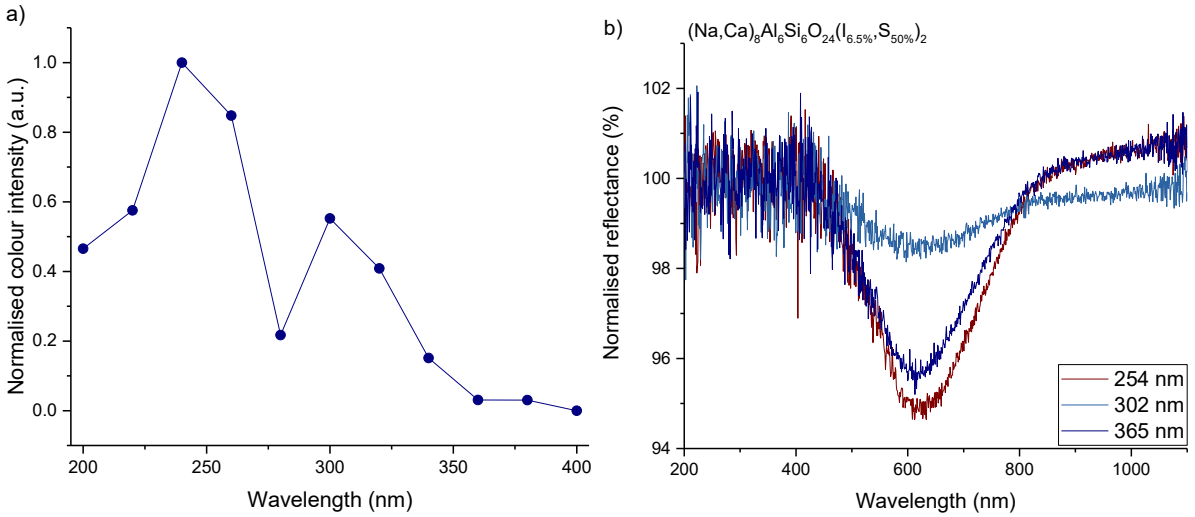

Figure 20. a) Photochromism excitation spectrum of $(Na,Ca)_8Al_6Si_6O_{24}(I_{6.6\%},S_{50\%})_2$ sample and reflectance spectra remeasured using the irradiation time of 10 min.

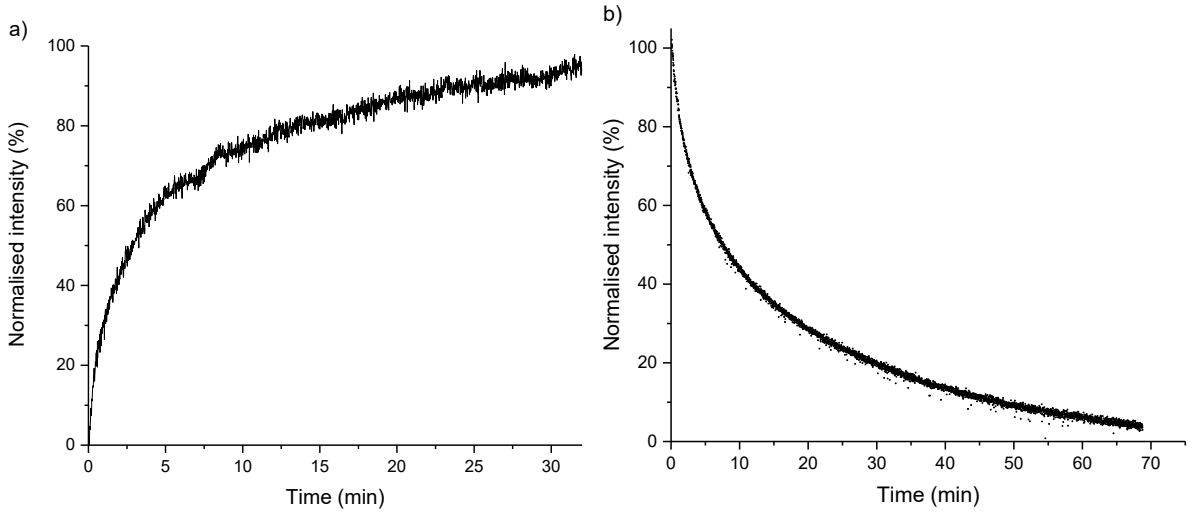

Figure 21. a) Photochromism rise curve and b) fade curve of $(Na,Ca)_8Al_6Si_6O_{24}(I_{6.6\%},S_{100\%})_2$ sample.

The PL properties of these samples were assessed to similar manner as previous samples, but only $(Na,Ca)_8Al_6Si_6O_{24}(Cl_{10\%},S_{100\%})_2$ exhibited luminescence, but as can be seen from the emission spectra (**Figure 22**), the emission intensity is weak. When photographed under 254 nm excitation, this sample shows unevenly distributed blue and orange emitting particles. The blue particles are most likely caused by Ti^{4+}, like in $(Na,K)_8Al_6Si_6O_{24}(I_{10\%},S_{100\%})_2$, which creates this broad left shoulder in the spectrum. The orange particles could be the combination of impurity Fe^{3+} ions and $S_2^{\bullet-}$. The heating was done in air which led to some compounds being oxidised, most likely some Fe^{2+} returning to Fe^{3+}. This caused the orange emission to improve, while the blue particles decreased. This indicates

that certain oxidation states work better in this cancrinite sample. It should also be kept in mind that the other phases could cause or contribute to the properties as well. Calcium silicate is known to be able host ions that can cause yellow-orange or red emission.[60,61] The properties of lawsonite have not been extensively explored yet, but the structure could be accommodating for colour centres with certain ions and defects. The $FeTiO_3$ could form small luminescent cluster, which would contribute to the emission particles.

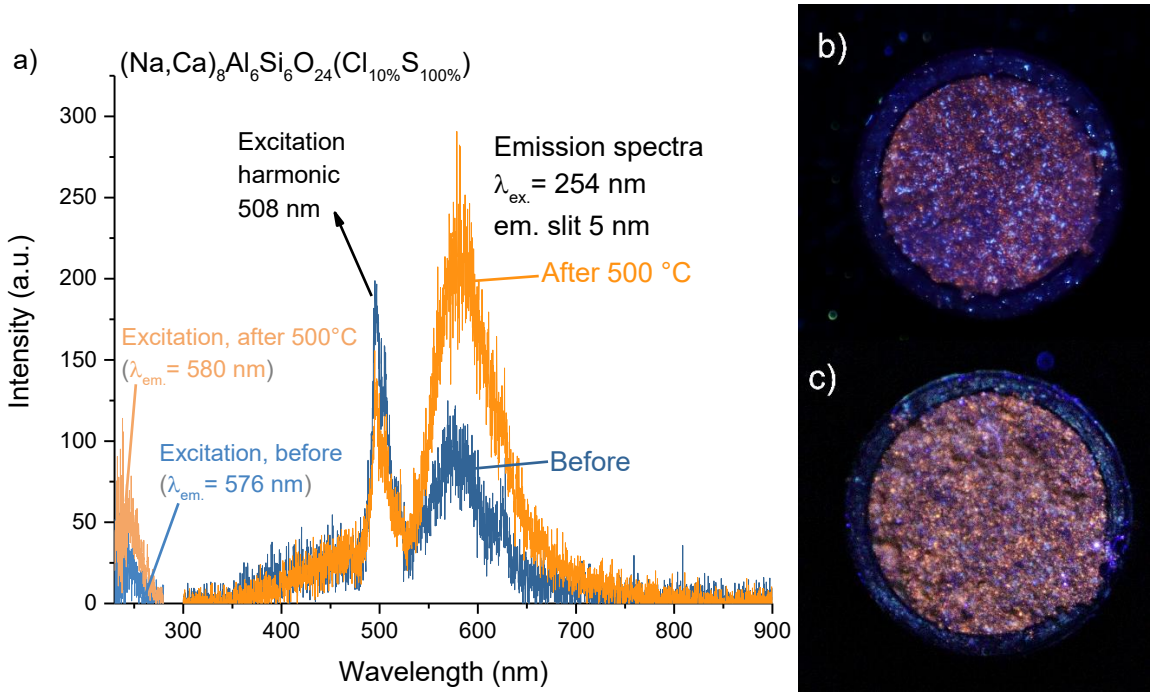

Figure 22. a) Excitation and emission spectra (excitation harmonic at 508 nm) of $(Na,Ca)_8Al_6Si_6O_{24}(Cl_{10\%},S_{100\%})_2$ b) Photos under 254 nm excitation before and c) after heating to 500 ℃ for an hour. Contrast and brightness have been adjusted to show the emission colors better

The BSE image (**Figure 23**) shows medium sized particles as well as a few larger ones containing heavier atoms that form their own phase. These larger particles seem to be made up of the same elements with some heavier atoms. Otherwise, the sample contains 2-3 µm hexagonal cancrinite particles.

A SEM-EDS elemental mapping (**Figure 24**) of $(Na,Ca)_8Al_6Si_6O_{24}(Cl_{10\%},S_{100\%})_2$ was done to show the elemental distribution between the two phases, as well as some other identified by PXRD. The sample consisted larger Ca-rich sheets with silicon and oxygen. Three of the Ca-rich particles have titanium with some iron in them. Since the larger sheets are depleted of aluminium and sodium, the most likely phases are lawsonite and calcium silicate. The smaller particles contain sodium, aluminium, silicon, oxygen, chlorine and sulphur indicating to cancrinite phase. The presence sulphur is mostly even throughout the sample, but some concentrated areas can be also seen. The concentrated sulphur areas can be seen accompanied by calcium indicating CaS. The CaS particles could be causing some luminescence properties,

especially with the impurities found in the sample. CaS is known to act as a host for red-orange emitters.[62] With the oxidation of this compound into $CaSO_4$, the luminescence would improve in this sample like seen with the PL results.

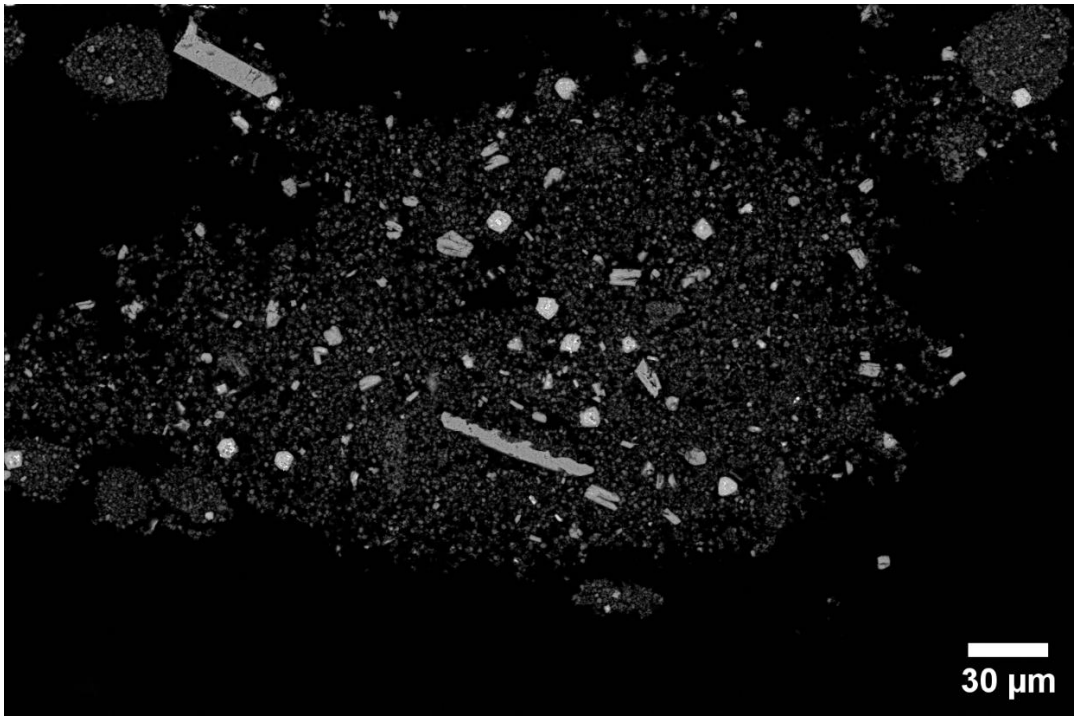

Figure 23. BSE image with 15 kV of $(Na,Ca)_8Al_6Si_6O_{24}(Cl_{10\%},S_{100\%})_2$ sample.

The amount of Cl atoms that ended up in the structure is unknown, since the epoxide used in the SEM-EDS measurements contained large amounts of chloride. Nonetheless, it can be seen that the Ca-rich areas do not contain chloride. Therefore, it can be concluded that little to no Cl atoms entered the structure.

A possible cause for the luminescence could be the $FeTiO_3$ particles. In addition to calcium, these particles are comprised of oxygen and some amounts of sodium and sulphur. While $FeTiO_3$ has not been reported to have luminescence itself, the chemical environment of this sample seems to be unusual, which could lead the $FeTiO_3$ particles to emit blue seen in the sample.

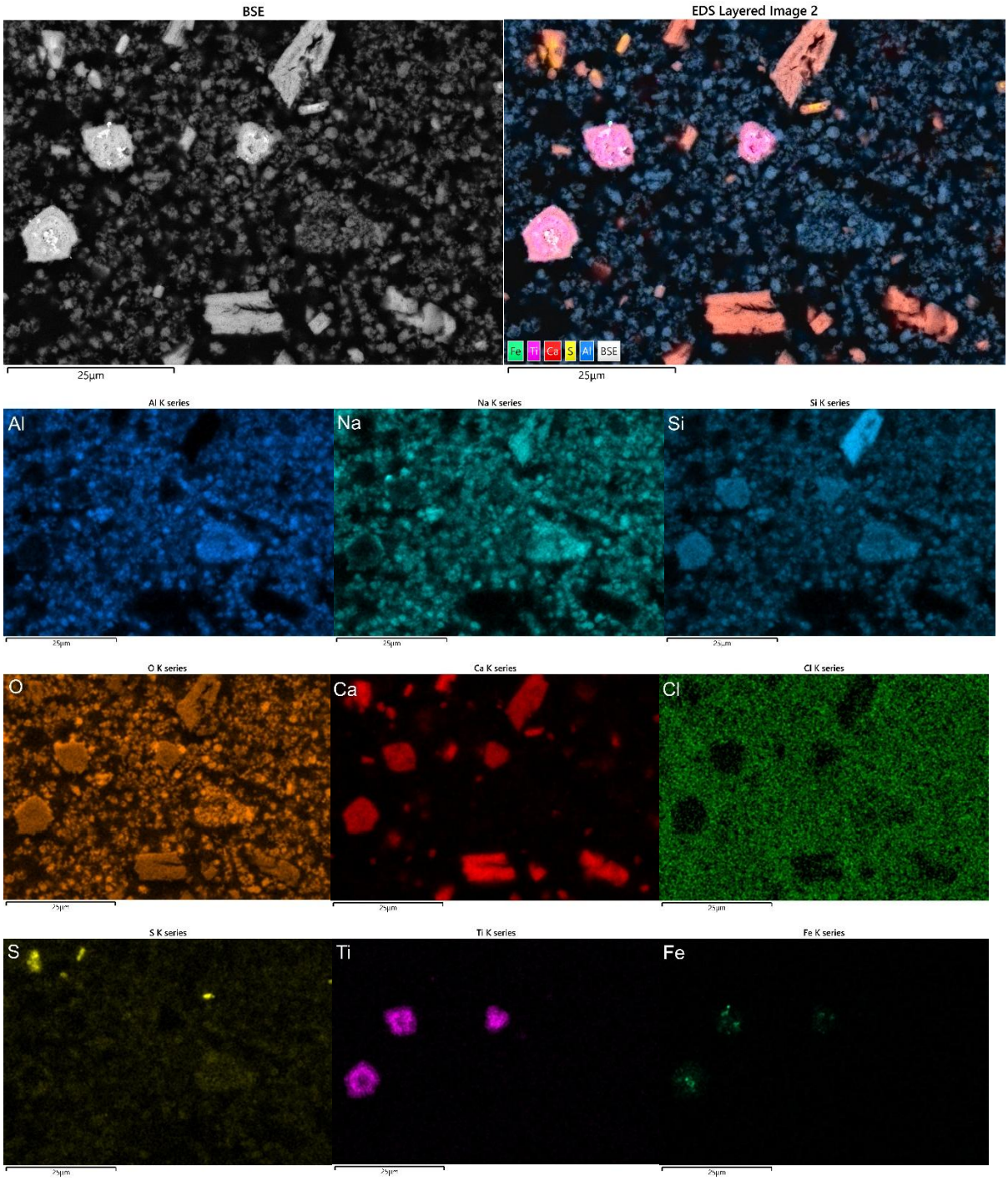

Figure 24. SEM-EDS elemental mapping using acceleration voltage of 15 kV of $(Na,Ca)_8Al_6Si_6O_{24}(Cl_{10\%},S_{100\%})_2$ sample.

A closer look at a titanium-rich particle (**Figure 25**) shows that the particle has even amounts of Si, Ca, and S atoms. Little to no Al atoms can be seen, which would indicate that some titanite has formed along with Fe. Titanite ($CaTiSiO_5$) has been shown to exhibit yellow to red-orange emission with Ce and Mn doping.[63] Although intentional addition of Mn was not done, some trace amounts was found in kaolin which could contribute to the optical properties. It is also possible the Fe acts as the orange emitters.

The SEM-EDS images show that cancrinite formed correctly with chloride despite the impurity phases and is prevailing. The same kaolin impurities persist, but in this sample the Fe atoms are more concentrated in alongside with Ti. The orange luminescence appears to be a mix of CaS, $CaSO_4$, and the titanite particles mixed with some impurity ions enabling the luminescence. The cancrinite particles do not contain calcium, which could be due to the sample still having large amounts of sulphur. The lack of calcium could also be because the Cl atoms stabilise the structure not allowing charge imbalanced ions to enter.

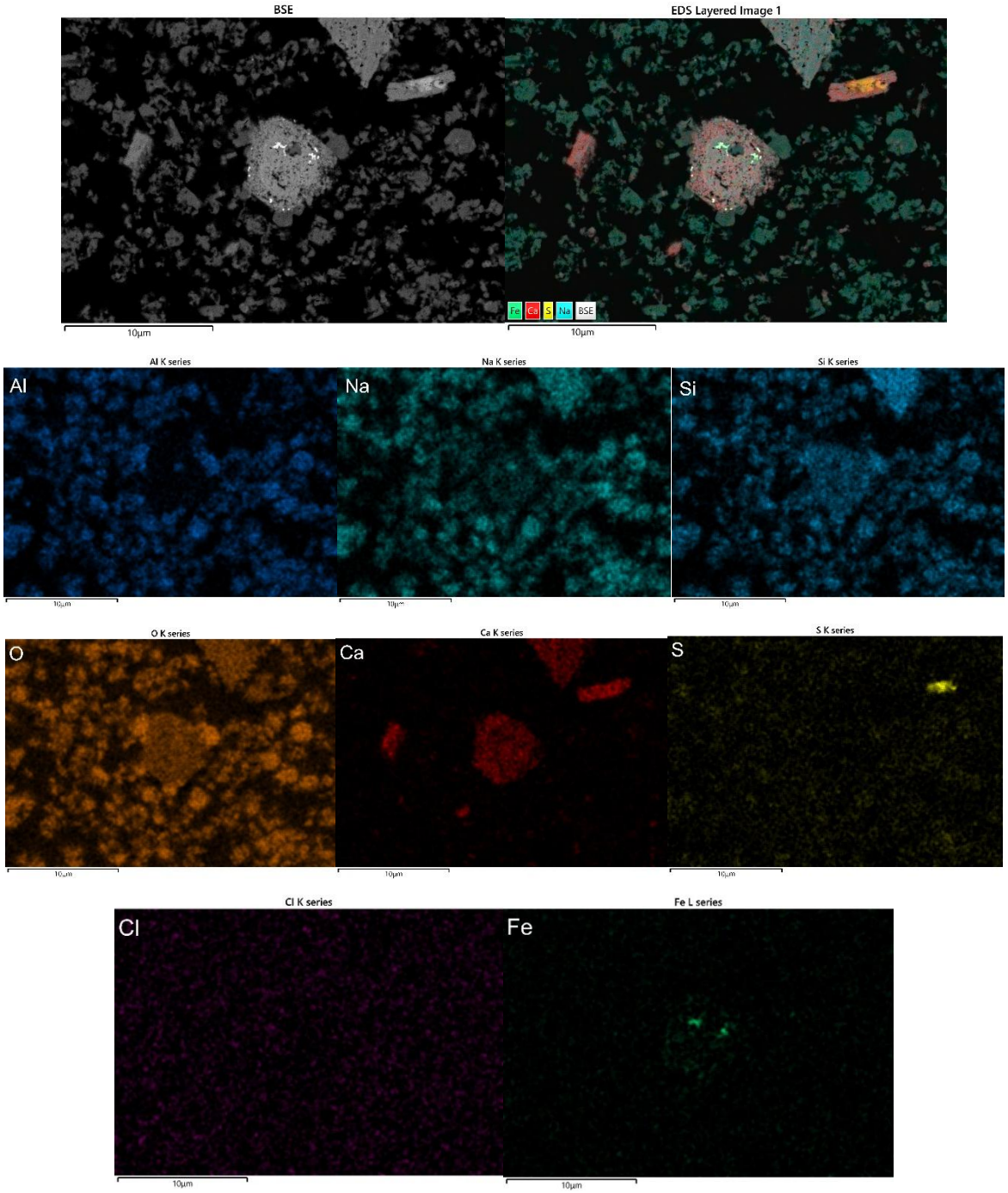

Figure 25. SEM-EDS elemental mapping on the titanium rich particles using acceleration voltage of 7 kV of $(Na,Ca)_8Al_6Si_6O_{24}(Cl_{10\%},S_{100\%})_2$.

3.6 Other measurements and tests

3.6.1 Thermoluminescence

Due to some samples exhibiting luminescence, more measurements were done. The TL measurements were performed on all samples, but only the ones showing some intensities are shown in **Figure 26**. With TL measurements, it was possible to assess the electron trap depth and estimate amount of them, when the sample was excited with UV and X-rays. Only a few samples produced a glow curve when exciting with 254 nm for 5 min. The UV excited samples produced a broad peak from 100 to 350 °C, but at very low intensities. The sample with clear intensity is $(Na,Ca)_8Al_6Si_6O_{24}(Cl_{10\%},S_{100\%})_2$. Although, the glow curve intensity is still low, it indicates to some number of traps with wide range of release energies, most centred around 200 °C.

The X-ray irradiated samples produced a clearer shape in most samples around 300 °C. The reason for this higher energy need could be the cleaner structure. The monovalent ions, especially when the structure is saturated with S^{2-} ions, leave less room for defects compared to the used divalent cation. This is especially apparent in the samples containing only sodium salts or with low substitution concentration. The lack of dissimilarity would create insufficient complexity of the defects thus creating shallow and negligible number of traps.

Only two samples, $(Na,Ca)_8Al_6Si_6O_{24}(Cl_{10\%},S_{100\%})_2$ and $(Na,Ca)_8Al_6Si_6O_{24}(I_{6.5\%},S_{50\%})_2$, had clear peaks at 243 and 227 °C, respectively. This is especially apparent in $(Na,Ca)_8Al_6Si_6O_{24}(Cl_{10\%},S_{100\%})_2$ sample. With divalent cation, the defects are more intricate leading to increased number of deeper traps. Although, the traps got released at relatively low temperatures, the broadness indicates traps getting released over a wide energy spectrum. Another reason for the increased number of traps could be the other, impurity phases which could have a lattice suitable for trapping centres combined with cancrinite structure.

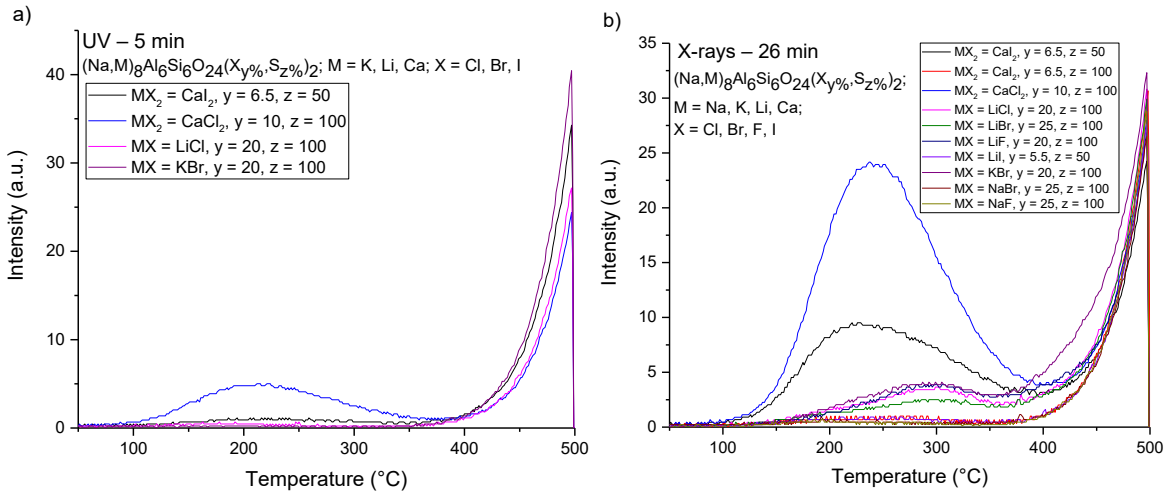

Figure 26. TL glow curves of samples excited with a) UV for 5 min and b) X-rays for 26 min.

3.6.2 OSL and X-ray imaging

Although the glow curve intensity of $(Na,Ca)_8Al_6Si_6O_{24}(Cl_{6.5\%},S_{100\%})_2$ sample was still low, a film was tape cast of the sample. The OSL was measured of this film to see if any signal could be obtained. In **Figure 27**, a slight signal was obtained using 635 nm red laser for stimulation. OSL was performed by exciting the film with 254 nm for 5 min and X-rays for 26 min (**Table 4**), but only X-ray excited measurement produced a clear signal which is presented in this study. This meant a possible image could be obtained using a dental imaging plate reader with X-ray excitation for 26 min. The acquired result obtained using XRF device excitation for 26 min and no imaged specimen (**Figure 27**) shows black dots that work as imaging material. These dots store more energy from the X-rays which creates trapped electrons. The electrons get released by the laser causing radiative recombination. The dots could be possibly linked to the different phases in this sample, especially the luminescence centres, which let the X-rays pass freely. Although, the black dots work better as imaging material, the grey areas also emit, but to a lesser extent.

It can be concluded from these results that some Na,Ca-CAN sample could work as OSL imaging material, but since the main phases in $(Na,Ca)_8Al_6Si_6O_{24}(Cl_{10\%},S_{100\%})_2$ sample were hydroxycancrinite and lawsonite, it cannot be said, what is causing the luminescence or the suitable properties for dental imaging. Neither material has yet to be studied regarding dental imaging.

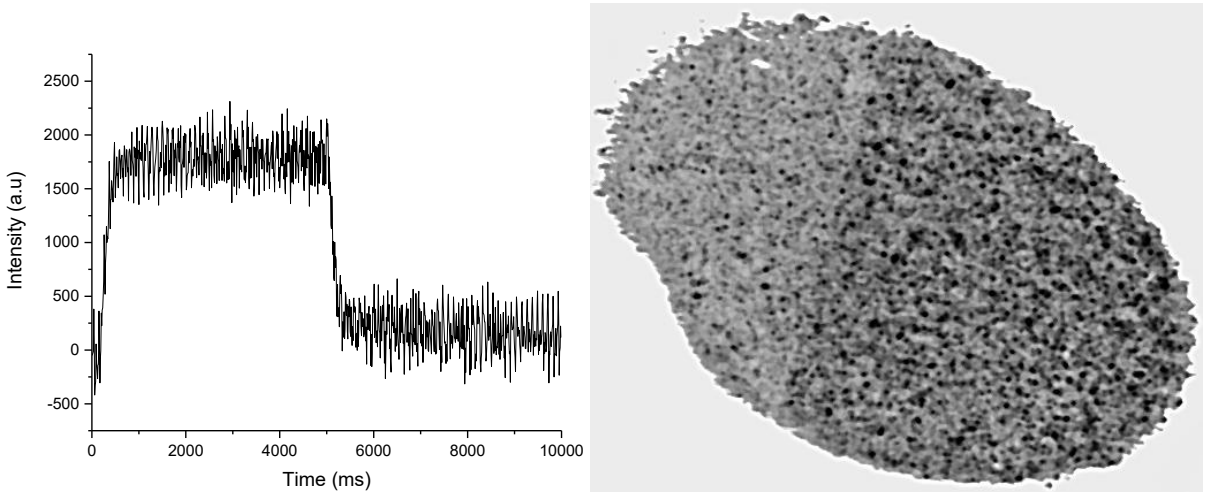

Figure 27. OSL spectrum of the obtained signal (left) and dental X-ray imaging result (right)

3.6.3 Effect of heat treatment on photochromism

To see if heating a sample to 500 °C for an hour would enhance the photochromic property or bleach the initial colour of the sample. Samples which had two absorbance minima before irradiation or minimal photochromic properties were chosen for the heating treatment. The samples were also chosen so that each cationic substitution was represented to examine, if the change in cation enables certain mechanisms.

The samples before heating and irradiation (**Figure 28**) show two absorbance minima at 470-500 and 700-740 nm depending on the sample. The sample $(Na,K)_8Al_6Si_6O_{24}(I_{10\%},S_{100\%})_2$ being an outlier and having the absorbance minima at 510 and 635 nm with the minima being less obvious. The cause for these two absorbance bands is unknown, but they could be related to cancrinite already having structural defects as well as the free S-radicals. The absorbance band at lower wavelengths seems to be related to kaolin having its own sharp absorbance minimum at 505 nm which slightly deepens upon 254 nm irradiation as well as some photochromic properties due to the impurities (**Figure S5a**). This shape correlation is more apparent in certain samples, e.g. $(Na,Li)_8Al_6Si_6O_{24}(Cl_{20\%},S_{100\%})_2$ sample has similar shape with the irradiated spectrum with more depth (**Figure S5b**) which most likely due to the different structure and increased number of defects. The difference curve shows the absorbance band being 560-650 nm depending on the sample, excluding $(Na,K)_8Al_6Si_6O_{24}(I_{10\%},S_{100\%})_2$ sample which has insignificant photochromic response. Notably, $Na_8Al_6Si_6O_{24}(Cl_{20\%},S_{75\%})_2$ sample has the strongest photochromic property with the minimum being at 646 nm.

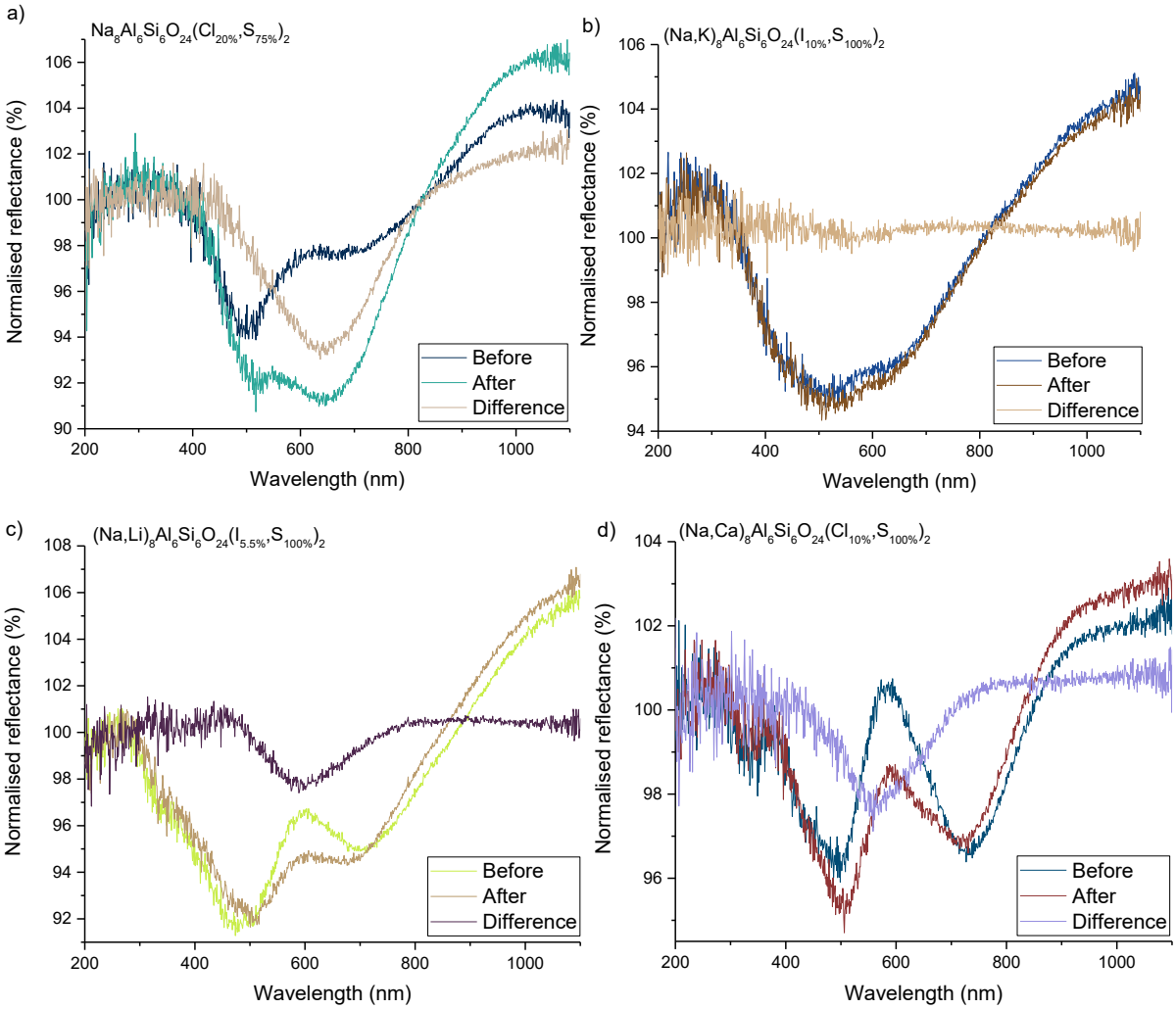

Figure 28. Reflectance spectra of a) $Na_8Al_6Si_6O_{24}(Cl_{20\%},S_{75\%})_2$, b) $(Na,K)_8Al_6Si_6O_{24}(I_{10\%},S_{100\%})_2$, c) $(Na,Li)_8Al_6Si_6O_{24}(I_{5.5\%},S_{100\%})_2$, and d) $(Na,Ca)_8Al_6Si_6O_{24}(Cl_{10\%},S_{100\%})_2$ samples before irradiation and after 254 nm irradiation for 5 min with their difference curves. These are measured before the additional heat treatment at 500 °C.

After the heat treatment, all samples exhibited the similar shape prior to irradiation. In $(Na,K)_8Al_6Si_6O_{24}(I_{10\%},S_{100\%})_2$ and $(Na,Ca)_8Al_6Si_6O_{24}(Cl_{10\%},S_{100\%})_2$ samples, the absorbance band before irradiation at 510 nm has deepened while the secondary minimum has disappeared. The similar effect can be seen in $Na_8Al_6Si_6O_{24}(Cl_{20\%},S_{75\%})_2$ and $(Na,Li)_8Al_6Si_6O_{24}(I_{5.5\%},S_{100\%})_2$ samples, where the first absorbance minimum has deepened slightly, but the second minimum has stayed the same. The changes after irradiation are similar across all four samples. The minimum being at 510-530 nm. In most samples, this causes no changes in the position of the difference minimum, but in $Na_8Al_6Si_6O_{24}(Cl_{20\%},S_{75\%})_2$, the minimum of the difference curve has shifted to 584 nm.

The changes in the reflectance spectra could be due to some compound oxidising, since the heat treatment was done in air. The most likely compound to oxidise, along with iron, are titanium and sulphide. Further investigations could be performed by measuring FT-IR. The

minor changes affect the shape and position of the absorption band. While the structural changes were not visible on PXRD diffractograms, the shape before and after irradiation start to resemble more kaolin. The decomposition of kaolin can start around 500 °C[64,65], which was also tested for the used kaolin, but will not be analysed further in this study. Although cancrinite can withstand higher temperatures without decomposing or changing phases, kaolin losing its stability in high temperatures can indicate the second heat treatment causing minor changes in the structure.

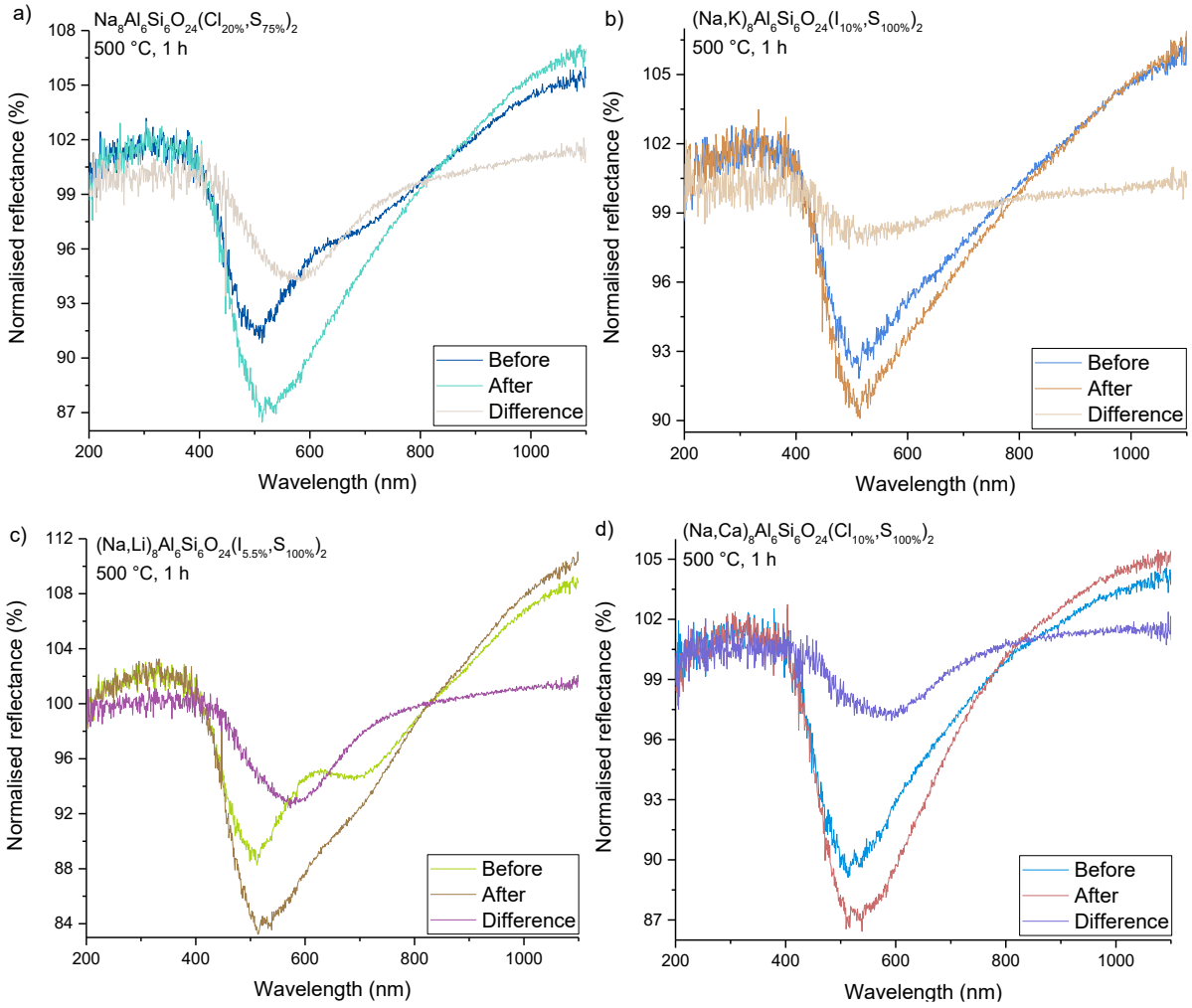

Figure 29. Reflectance spectra of samples a) $Na_8Al_6Si_6O_{24}(Cl_{20\%},S_{75\%})_2$, b) $(Na,K)_8Al_6Si_6O_{24}(I_{10\%},S_{100\%})_2$, c) $(Na,Li)_8Al_6Si_6O_{24}(I_{5.5\%},S_{100\%})_2$, and d) $(Na,Ca)_8Al_6Si_6O_{24}(Cl_{10\%},S_{100\%})_2$ after heat treatment to 500 °C for an hour. The spectra consist of before irradiation and after 254 nm irradiation for 5 min with their difference curves.

4 Conclusions

The photochromic and luminescence properties of cancrinite were successfully uncovered by ion substitution based on all the results. The synthesis of different cancrinite variants with different anions in most samples produced a cancrinite phase. Although the effectivity of the substitution is still uncertain, the properties indicate a small amount was able to enter the structure. Each salt caused the properties to differ slightly. The photochromism was weak across all samples, but two samples prevailed, $Na_8Al_6Si_6O_{24}(Cl_{10\%},S_{75\%})_2$ and $(Na,Ca)_8Al_6Si_6O_{24}(I_{6.5\%},S_{50\%})_2$. These samples exhibited photochromism that turned grey upon UV irradiation, and these samples also exhibited rise and fade properties of photochromism similar to hackmanite. Additionally, the colouring cycle of these samples might differ from hackmanite but would need further investigation.

The PL properties of the samples were weak, but in $(Na,K)_8Al_6Si_6O_{24}(I_{10\%},S_{100\%})_2$ and $(Na,Ca)_8Al_6Si_6O_{24}(Cl_{10\%},S_{100\%})_2$, the luminescence was created in individual emitting blue or orange. From the PL results, it can be also seen that some impurity Eu^{3+} ions were able to integrate into the structure. Although embedding Eu ions was not intended, their presence shows that cancrinite acts as a host for many guest ions. With intentional luminescent ion incorporation, cancrinite could be found to be suitable for creating different luminescence properties.

The impurities found in kaolin, titanium and iron, can forbid the substitution and some properties e.g. luminescence. The possible effect of these ions was seen in the properties, especially in the PL spectra. The effect of these impurity ions on photochromism is unknown and requires more experiments. However, the inclusion of these ions was not adequate enough to cause the properties to excel. Another ion blocking the substitution could be S^{2-} ions, since the amount of Na_2SO_4 used during the synthesis was enough to saturate the structure with S^{2-} ions. This could lead to less desired anions to enter the structure, or the cations would form other compounds deriving the cancrinite structure of sulphide.

The samples with decreased amounts of Na_2SO_4 also gave valuable information on the behaviour of the structure. The ions substitution did not behave in an expected way, but with changing the Na_2SO_4 amount, some ions were incorporated with less difficulty than others. With this better ratio can be found.

The samples including Cl were exhibiting the strongest photochromism in almost all sample batches, except Na,Ca-CAN. The results suggest that for photochromism in cancrinite, the substitution ion needs to be similar size, what there is already in the structure. In this case

it was S^{2-} ion which are similar sized as Cl^{-} ions. The reason for $(Na,Ca)_8Al_6Si_6O_{24}(Cl_{10\%},S_{100\%})_2$ lacking the photochromic response could be due to the different phases found in the sample. With more trials, it can be studied if purer product can be obtained. It is also worth noting that in some cases obtaining better photochromic response, higher energy irradiation might be needed. Samples with large ions, like iodide, might need X-rays to enhance the colour change. With more research and tuning, the properties of cancrinite can be revealed to exhibit strong photochromism and luminescence. With the discoveries, more application can be uncovered, considering that cancrinite has potential in sensing.

References

1. Buhl, J. C. & Petrov, V. The Hydrothermal Synthesis of Sulfate Cancrinite (SO_4-CAN): Relations Between Si-Al Sources and Crystal Quality. *Zeitschrift für Anorganische und Allgemeine Chemie* **645**, 1229–1239 (2019).
2. Wernert, V., Schaef, O., Aloui, L., Chassigneux, C., Ayari, F., Ben Hassen Chehimi, D. & Denoyel, R. Cancrinite Synthesis from Natural Kaolinite by High Pressure Hydrothermal Method: Application to the Removal of Cd^{2+} and Pb^{2+} from Water. *Microporous and Mesoporous Materials* **301**, (2020).
3. Hassan, I. & Grtindy, H. D. The Crystal Structure of Basic Cancrinite, Ideally $Na_8[Al_6Si_6O_{24}](OH_2)\cdot 3H_2O$. *Canadian Mineralogist* **29**, 377–383 (1991).
4. Chukanov, N. V., Aksenov, S. M. & Rastsvetaeva, R. K. Structural Chemistry, IR Spectroscopy, Properties, and Genesis of Natural and Synthetic Microporous Cancrinite- and Sodalite-Related Materials: A Review. *Microporous and Mesoporous Materials* **323**, (2021).
5. Shendrik, R., Kaneva, E., Radomskaya, T., Sharygin, I. & Marfin, A. Relationships Between the Structural, Vibrational, and Optical Properties of Microporous Cancrinite. *Crystals* **11**, (2021).
6. Ralph, J., Von Bargen, D., Martynov, P., Zhang, J., Que, X., Prabhu, A., Morrison, S. M., Li, W., Chen, W. & Ma, X. Cancrinite: Mineral information, data and localities. *Mindat.org: The open access mineralogy database to accelerate data-intensive geoscience research. American Mineralogist, 110(6)* 833–844 https://www.mindat.org/min-880.html (2025) doi:10.2138/am-2024-9486. (Accessed 24/03/2026)
7. Buck, E. C. & McNamara, B. K. Precipitation of Nitrate-cancrinite in Hanford Tank Sludge. *Environmental Science and Technology* **38**, 4432–4438 (2004).
8. Jarchow, O. Atomanordnung und Strukturverfeinerung von Cancrinit. *Zeitschrift für Anorganische und Allgemeine Chemie* **122**, 407–422 (1965).
9. Pauling, L. The Structure of Some Sodium and Calcium Aluminosilicates. *Proceedings of the National Academy of Sciences* **16**, (1930).
10. Colmenares-Zerpa, J., Dugarte-Dugarte, A., Delgado, J. M. & Rodríguez-Sulbarán, P. Preparation and Characterization of Sulfate Cancrinite, a Synthetic Analog of Vishnevite, Obtained Under Mild Hydrothermal Conditions. *Next Materials* **9**, (2025).
11. Chukanov, N. V., Nedelko, V. V., Blinova, L. N., Korshunova, L. A., Olysych, L. V., Lykova, I. S., Pekov, I. V., Buhl, J. C. & Depmeier, W. The Role of Additional Anions in Microporous Aluminosilicates with Cancrinite-type Framework. *Russian Journal of Physical Chemistry B* **6**, 593–600 (2012).
12. Weller, M. T. & Kenyon, N. J. Investigation of Cancrinite Structures by Powder Neutron Diffraction. *Studies in Surface Science and Catalysis* **154**, 1349–1355 (2004).

13. K. Hackbarth, Th.M. Gesing, M. Fechtelkord, F. Stief & J.-Ch. Buhl. Synthesis and Crystal Structure of Carbonate Cancrinite $Na_8[alsio_4]_6co_3(H_2o)_{3.4}$, Grown Under Low-temperature Hydrothermal Conditions. *Microporous and Mesoporous Materials* **30**, 347–358 (1999).
14. Deng, Y., Flury, M., Harsh, J. B., Felmy, A. R. & Qafoku, O. Cancrinite and Sodalite Formation in the Presence of Cesium, Potassium, Magnesium, Calcium and Strontium in Hanford Tank Waste Simulants. *Applied Geochemistry* **21**, 2049–2063 (2006).
15. Wang, H., Zhang, F., Ang, R. & Ren, D. Hydrothermal Synthesis of Cancrinite from Coal Gangue for the Immobilization of Sr. *Materials* **17**, (2024).
16. Hoffmann, S. K., Goslar, J., Lijewski, S., Olejniczak, I., Jankowska, A., Zeidler, S., Koperska, N. & Kowalak, S. S_3^- radicals in ε-cages of Cancrinite and Zeolite L: Spectroscopic and Magnetic Resonance Studies. *Microporous and Mesoporous Materials* **151**, 70–78 (2012).
17. Liu, Q., Xu, H. & Navrotsky, A. Nitrate Cancrinite: Synthesis, Characterization, and Determination of the Enthalpy of Formation. *Microporous and Mesoporous Materials* **87**, 146–152 (2005).
18. Moreno-Torres, J. A., Flores-Acosta, M., Ramírez-Bon, R. & Coutino-Gonzalez, E. Lead Confinement and Fluorimetric Detection Using Zeolites: Towards a Rapid and Cost-effective Detection of Lead in Water. *JPhys Photonics* **3**, (2021).
19. Mintova, S., Jaber, M. & Valtchev, V. Nanosized Microporous Crystals: Emerging Applications. *Chemical Society Reviews* **44**, 7207–7233 (2015).
20. Chukanov, N. V., Vigasina, M. F., Shendrik, R. Y., Varlamov, D. A., Pekov, I. V. & Zubkova, N. V. Nature and Isomorphism of Extra-Framework Components in Cancrinite-and Sodalite-Related Minerals: New Data. *Minerals* **12**, (2022).
21. Xu, B., Smith, P., Wingate, C. & De Silva, L. The Effect of Calcium and Temperature on the Transformation of Sodalite to Cancrinite in Bayer Digestion. *Hydrometallurgy* **105**, 75–81 (2010).
22. Mon, J., Deng, Y., Flury, M. & Harsh, J. B. Cesium Incorporation and Diffusion in Cancrinite, Sodalite, Zeolite, and Allophane. *Microporous and Mesoporous Materials* **86**, 277–286 (2005).
23. Pekov, I. V., Olysych, L. V., Chukanov, N. V., Zubkova, N. V., Pushcharovsky, D. Y., Van, K. V., Giester, G. & Tillmanns, E. Crystal Chemistry of Cancrinite-group Minerals With an *AB*-type Framework: A Review and New Data. I. Chemical and Structural Variations. *Canadian Mineralogist* **49**, 1129–1150 (2011).
24. Miyake, M., Akachi, T. & Matsuda, M. Preparation, Structure and Photocatalytic Properties of Cancrinite Encapsulating Lead and Sulfide Ions. *Journal of Materials Chemistry* **15**, 791–797 (2005).
25. Norrbo, I., Curutchet, A., Kuusisto, A., Mäkelä, J., Laukkanen, P., Paturi, P., Laihinen, T., Sinkkonen, J., Wetterskog, E., Mamedov, F., Le Bahers, T. & Lastusaari, M. Solar UV Index

and UV Dose Determination with Photochromic Hackmanites: From the Assessment of the Fundamental Properties to the Device. *Materials Horizons* **5**, 569–576 (2018).

26. Yamaguchi, T. & Ogawa, M. Photochromic Reactions in Nanospace: Host–Guest Interactions and Opportunity. in *Chemistry of Silica and Zeolite-Based Materials: Synthesis, Characterization and Applications* vol. 2 163–177 (Elsevier, 2019).
27. He, T. & Yao, J. Photochromism in Composite and Hybrid Materials Based on Transition-metal Oxides and Polyoxometalates. *Progress in Materials Science* **51**, 810–879 (2006).
28. Kaneva, E. & Shendrik, R. Radiation Defects and Intrinsic Luminescence of Cancrinite. *Journal of Luminescence* **243**, (2022).
29. Yang, R., Chen, L., Lin, C., Huang, H., Wu, Z., Zhan, C., Zhuang, Y. & Xie, R. J. Relationship Between Photochromism and Persistent Luminescence in Barium-magnesium Silicates. *Chemical Engineering Journal* **493**, (2024).
30. Vuori, S., Colinet, P., Norrbo, I., Steininger, R., Saarinen, T., Palonen, H., Paturi, P., Rodrigues, L. C. V., Göttlicher, J., Le Bahers, T. & Lastusaari, M. Detection of X-ray doses with color-changing hackmanites: Mechanism and application. *Advanced Optical Materials* **9**, 1–13 (2021).
31. Colinet, P. & Le Bahers, T. Engineering Aluminosilicate's Photochromism by Quantum Chemistry. *Journal of Materials Chemistry C* **11**, 730–741 (2022).
32. Williams, E. R., Simmonds, A., Armstrong, J. A. & Weller, M. T. Compositional and Structural Control of Tenebrescence. *Journal of Materials Chemistry* **20**, 10883–10887 (2010).
33. Norrbo, I., Carvalho, J. M., Laukkanen, P., Mäkelä, J., Mamedov, F., Peurla, M., Helminen, H., Pihlasalo, S., Härmä, H., Sinkkonen, J. & Lastusaari, M. Lanthanide and Heavy Metal Free Long White Persistent Luminescence from Ti Doped Li–Hackmanite: A Versatile, Low-Cost Material. *Advanced Functional Materials* **27**, (2017).
34. Williams, E. F., Hodgson, W. G. & Brinen, J. S. Synthetic Photochromic Sodalite. *Journal of the American Ceramic Society* **52**, 139–144 (1969).
35. Phillips, W. Properties of Cathodochromic Sodalite. **117**, 1558–1561 (1970).
36. Apopei, A. I. & Aștefanei, D. First Report of Fluorescent Sodalite from the Ditrău Alkaline Massif, Romania: A Mineralogical and Spectroscopic Investigation. *Minerals* **15**, (2025).
37. Shibaeva, D. N., Kompanchenko, A. A., Bulatov, V. V. & Asanovich, D. A. Express Assessment of Apatite Content in Apatite–Nepheline Ores of Ultrabasic Alkaline Complexes Based on Its Luminescent Properties (The First Study Stage). *Minerals* **13**, (2023).
38. Ralph, J., Von Bargen, D., Martynov, P., Zhang, J., Que, X., Prabhu, A., Morrison, S. M., Li, W., Chen, W. & Ma, X. Kyanoxalite: Mineral information, data and localities. *Mindat.org: The open access mineralogy database to accelerate data-intensive geoscience research. American Mineralogist, 110(6)* 833–844 https://www.mindat.org/min-38989.html (2025) doi:10.2138/am-2024-9486. (Accessed 24/03/2026)

39. Bogdanov, A. I., Chukanov, N. V., Shendrik, R. Y. & Pekov, I. V. Spectroscopic Properties of Polysulfide Anions, Radical Anions, and Molecules: Ab Initio Calculations and Application to Minerals of the Sodalite and Cancrinite Groups. *Minerals* **15**, (2025).
40. Garcia-Guinea, J., Correcher, V., Sanchez-Muñoz, L., Finch, A. A., Hole, D. E. & Townsend, P. D. On the Luminescence Emission Band at 340 Nm of Stressed Tectosilicate Lattices. *Nuclear Instruments and Methods in Physics Research, Section A: Accelerators, Spectrometers, Detectors and Associated Equipment* **580**, 648–651 (2007).
41. Chukanov, N. V., Shchipalkina, N. V., Shendrik, R. Y., Vigasina, M. F., Tauson, V. L., Lipko, S. V., Varlamov, D. A., Shcherbakov, V. D., Sapozhnikov, A. N., Kasatkin, A. V., Zubkova, N. V. & Pekov, I. V. Isomorphism and Mutual Transformations of S-Bearing Components in Feldspathoids with Microporous Structures. *Minerals* **12**, (2022).
42. Ouarab, N., Benharrat, L., Redjdal, N., Mezghiche, S., Manseri, A. & Toumert, I. Photoluminescence Properties of Modified Kaolin Ceramic in Response to UV Irradiation. *Radiation Physics and Chemistry* **237**, (2025).
43. International Centre for Diffraction Data, PDF-4+ 2024, entries 04-012-0446 (cancrinite), 04-008-4863 (sodalite), 01-078-2494 (hydroxycancrinite), 04-012-1686 (lawsonite), 04-011-6361 ($CaO{\cdot}SiO_4$), 04-013-3472 ($FeTiO_3$).
44. Pauling, L. *The Nature of the Chemical Bond*. *Zeitschrift für Kristallographie Crystalline Materials* (Cornell University Press, 1960).
45. Song, C., Guo, Q., Liu, Y., Rao, Y. & Liao, L. Photochromism, UV-Vis, Vibrational and Fluorescence Spectroscopy of Differently Colored Hackmanite. *Crystals* **13**, (2023).
46. Colinet, P., Gheeraert, A., Curutchet, A. & Le Bahers, T. On the Spectroscopic Modeling of Localized Defects in Sodalites by TD-DFT. *Journal of Physical Chemistry C* **124**, 8949–8957 (2020).
47. Page, P. S., Dhabekar, B. S., Bhatt, B. C., Dhoble, A. R. & Godbole, S. V. Role of Ti^{4+} In the Luminescence Process of Al_2O_3:Si,Ti. *Journal of Luminescence* **130**, 882–887 (2010).
48. Mehta, S. K. & Sengupta, S. Luminescence and Colour Centres in Al_2O_3:Si,Ti. *Nuclear Instruments and Metiiods* **164**, 349–354 (1979).
49. Ueda, M. & Ohtsuka, T. Luminescence From Band-gap Photo-excitation of Titanium Anodic Oxide Films. *Corrosion Science* **44**, 1633–1638 (2002).
50. Macke, A. J. H. Investigations on the Luminescence of Titanium-activated Stannates and Zirconates. *Journal of Solid State Chemistry* **18**, 337–346 (1976).
51. Gaft, M., Panczer, G., Nagli, L. & Yeates, H. Laser-induced Time-resolved Luminescence of Tugtupite, Sodalite and Hackmanite. *Physics and Chemistry of Minerals* **36**, 127–141 (2009).
52. Jin, Q., Wu, R., Pan, Y., Ding, Y., Lian, H., Lin, J. & Li, L. Dual-emissive Luminescence in OIHMH Single Crystals: Tunable Red-green Emissions via Mn^{2+} Doping and Theoretical Insights. *Chemical Science* **15**, 17173–17182 (2024).

53. Agamah, C., Vuori, S., Colinet, P., Norrbo, I., de Carvalho, J. M., Okada Nakamura, L. K., Lindblom, J., van Goethem, L., Emmermann, A., Saarinen, T., Laihinen, T., Laakkonen, E., Linden, J., Konu, J., Vrielinck, H., van der Heggen, D., Smet, P. F., Le Bahers, T., *et al.* Hackmanite - The Natural Glow-in-the-dark Material. *Chemistry of Materials* **32**, 8895–8905 (2020).

54. Khode, P. P., Deshmukh, A., Czerwiński, M., Michalska-Domańska, M. & Dhoble, S. J. Energy Transfer and Multicolour Photoluminescence in Phosphors La_2O_3 Doped by Tm^{3+}, Ho^{3+}, and Eu^{3+} for White LED and Security Applications. *Scientific Reports* **16**, (2026).

55. Geldasa, F. T., Etefa, H. F. & Dejene, F. B. Effect of Europium Doping on the Structural, Morphological, and Luminescent Properties of $Y_3Al_5O_{12}$ Phosphors Produced by Combustion Method. *Journal of Fluorescence* **35**, 10423–10430 (2025).

56. Kumarbekov, K. K., Kakimov, A. B., Karipbayev, Z. T., Kassymzhanov, M. T., Brik, M. G., Ma, C. geng, Piasecki, M., Suchikova, Y., Kemere, M. & Konuhova, M. Temperature-Dependent Luminescence of Europium-doped Ga_2O_3 Ceramics. *Optical Materials: X* **25**, (2025).

57. Norby P., Krogh Andersen E., Krogh Andersen I.G., Coella C. & de'Gennaro M. Synthesis and Structure of Lithium Cesium and Lithium Thallium Cancrinites. *Zeolites* **11**, 248–253 (1991).

58. Xiao, Y., Yang, X., Zhao, H. R., Wu, D., Chen, M. X., Zheng, T., Zhang, R., Sun, L. D. & Yan, C. H. Tracing the Origin of Near-infrared Emissions Emanating from Manganese (Ii). *Light: Science and Applications* **14**, (2025).

59. Paul Myrow. Colors of Sedimentary Rocks. in *Encyclopedia of Sediments and Sedimentary Rocks* (eds. Middleton, G. V., Church, M. J., Coniglio, M., Hardie, L. A. & Longstaffe, F. J.) 159–161 (Kluwer Academic Publishers, 2003).

60. Kojima, Y., Kamei, S. & Nishimiya, N. Preparation and Fluorescence Property of Red-emitting Eu^{3+}-activated Amorphous Calcium Silicate Phosphor. *Materials Research Bulletin* **45**, 121–123 (2010).

61. Kaur, H., Jayasimhadri, M., Sahu, M. K., Rao, P. K. & Reddy, N. S. Synthesis of Orange Emitting Sm^{3+} Doped Sodium Calcium Silicate Phosphor by Sol-gel Method for Photonic Device Applications. *Ceramics International* **46**, 26434–26439 (2020).

62. Ruelle, N., Pham-Thi, M. & Fouassier, C. Cathodoluminescent Properties and Energy Transfer in Red Calcium Sulfide Phosphors (CaS:Eu, Mn). *Japanese Journal of Applies Physics* 2786–2790 (1992).

63. Cao, R., Jiao, Y., Wang, X., Ouyang, X., Chen, T., Wan, H., Fan, T. & Xie, S. Tunable Emission Properties of $CaTiSiO_5$:Ce^{3+}, Mn^{2+} Phosphor via Efficient Energy Transfer. *Journal of Electronic Materials* **49**, 3869–3876 (2020).

64. Deju, R., Cucos, A., Mincu, M. & Tuca, C. Thermal Characterization of Kaolinitic Clay. *Romanian Journal of Physics* **66**, 904 (2021).

65. Dohnalová, Ž., Svoboda, L. & Šulcová, P. Characterization of Kaolin Dispersion Using Acoustic and Electroacoustic Spectroscopy. *Journal of Mining and Metallurgy, Section B: Metallurgy* **44**, 63–72 (2008).

Supporting Information

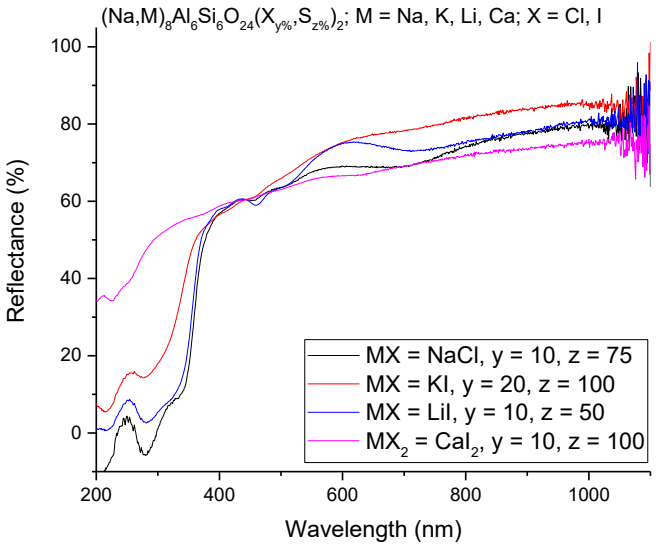

Figure S1. Reflectance spectra of various samples before irradiation.

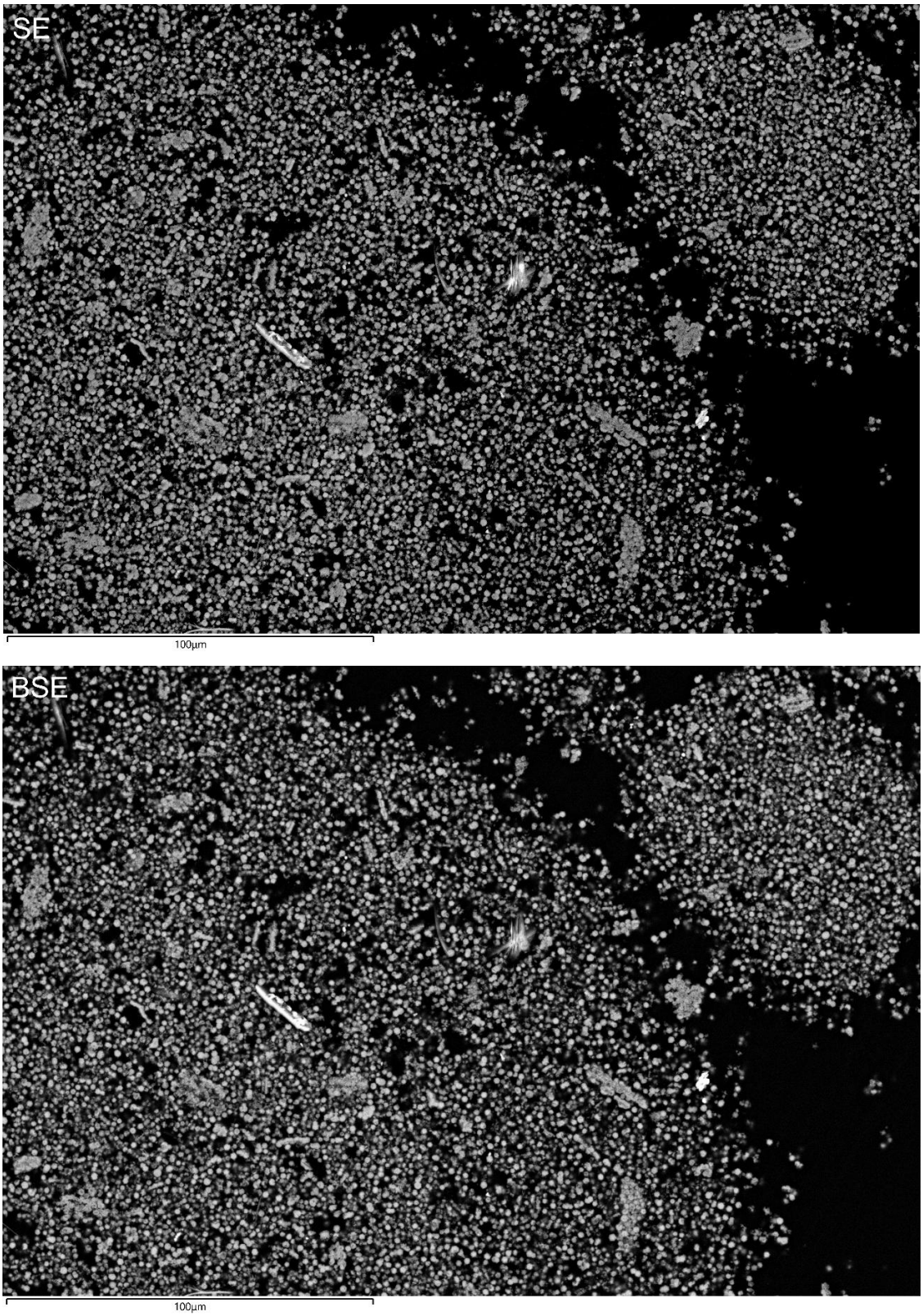

Figure S2. The SE (upper) and BSE imaging signals using acceleration voltage of 15 kV in SEM of $(Na,K)_8Al_6Si_6O_{24}(I_{10\%},S_{100\%})_2$.

Table S1. XRF results of the reduced Na-CAN samples.

Sample	Element (wt.%)												
	Na	Al	Si	S	Cl	K	Ca	Ti	Mn	Fe	Br	I	Eu
$Na_8Al_6Si_6O_{24}(Cl_{10\%},S_{75\%})_2$	9.45	30.28	44.27	9.45	2.75	1.55	0.14	0.87	0.004	1.05	0.16	-	0.03
$Na_8Al_6Si_6O_{24}(Cl_{20\%},S_{75\%})_2$	12.98	30.52	43.67	9.23	1.65	0.25	0.10	0.51	0.003	0.96	0.03	-	0.003
$Na_8Al_6Si_6O_{24}(Cl_{25\%},S_{100\%})_2$	12.69	30.40	43.45	9.17	1.73	0.29	0.14	0.96	0.01	1.08	0.09	-	-
$Na_8Al_6Si_6O_{24}(Cl_{30\%},S_{100\%})_2$	12.68	29.31	39.75	6.60	3.69	0.15	0.12	0.79	0.003	0.87	0.02	-	0.03
$Na_8Al_6Si_6O_{24}(Br_{25\%},S_{100\%})_2$	2.27*	29.53	46.58	10.23	2.90	3.21	-	1.10	0.00	1.24	2.93	-	0.02
$Na_8Al_6Si_6O_{24}(F_{25\%},S_{100\%})_2$	13.06	31.06	42.81	10.17	0.54	0.23	0.50	0.72	0.001	0.88	0.002	-	0.03
$Na_8Al_6Si_6O_{24}(I_{25\%},S_{100\%})_2$	16.79	30.94	40.48	9.32	0.49	0.17	0.08	0.64	0.009	1.01	-	0.08	-

* Indicates unreliable result

Table S2. XRF results of reduced Na,K-CAN samples

Sample	Element (wt.%)												
	Na	Al	Si	S	Cl	K	Ca	Ti	Mn	Fe	Br	I	Eu
$(Na,K)_8Al_6Si_6O_{24}(Cl_{20\%},S_{100\%})_2$	5.15	28.68	40.83	10.66	0.49	12.11	-	0.92	0.003	1.14	-	-	0.02
$(Na,K)_8Al_6Si_6O_{24}(Cl_{20\%},S_{50\%})_2$	7.97	29.42	32.65	11.34	0.22	5.96	-	1.19	0.01	1.20	-	0.03	-
$(Na,K)_8Al_6Si_6O_{24}(Br_{20\%},S_{100\%})_2$	5.27	28.33	50.06	11.73	0.14	0.17*	0.14	1.37	0.02	1.52	1.22	-	0.03
$(Na,K)_8Al_6Si_6O_{24}(I_{20\%},S_{100\%})_2$	6.47	28.35	40.48	10.47	0.24	11.72	-	0.93	0.02	1.13	-	0.10	-
$(Na,K)_8Al_6Si_6O_{24}(I_{20\%},S_{50\%})_2$	10.18	29.60	31.39	10.50	0.36	5.63	-	1.13	0.01	1.14	-	0.05	-
$(Na,K)_8Al_6Si_6O_{24}(I_{10\%},S_{100\%})_2$	3.96	28.12	30.56	10.74	0.29	13.88	-	1.18	0.01	1.14	-	0.10	0.00*

* Indicates unreliable result

Table S3. XRF results of reduced Na,Li-CANs.

Sample	Element (wt.%)												
	Na	Al	Si	S	Cl	K	Ca	Ti	Mn	Fe	Br	I	Eu
$(Na,Li)_8Al_6Si_6O_{24}(Cl_{20\%},S_{100\%})_2$	5.22	28.55	50.81	11.54	0.47	0.17	011	1.59	0.02	1.53	-	-	-
$(Na,Li)_8Al_6Si_6O_{24}(Br_{20\%},S_{100\%})_2$	4.87	27.88	51.49	11.19	0.16	0.16	0.18	1.49	0.01	1.66	0.89	-	0.03
$(Na,Li)_8Al_6Si_6O_{24}(F_{20\%},S_{100\%})_2$	10.41	28.32	58.19	9.61	0.54	0.18	0.16	1.24	0.02	1.34	-	-	-
$(Na,Li)_8Al_6Si_6O_{24}(I_{10\%},S_{100\%})_2$	5.91	30.80	46.80	12.36	0.57	0.22	0.15	1.76	0.02	1.42	-	-*	-
$(Na,Li)_8Al_6Si_6O_{24}(I_{10\%},S_{50\%})_2$	9.44	30.71	44.85	11.41	0.61	0.23	0.11	1.38	0.00	1.21	-	-*	0.003

* Indicates unreliable result

Table S4. XRF results of reduced Na,Ca-CANs.

Sample	Element (wt.%)											
	Na	Al	Si	S	Cl	K	Ca	Ti	Mn	Fe	I	Eu
$(Na,Ca)_8Al_6Si_6O_{24}(Cl_{10\%},S_{100\%})_2$	1.06	18.48	24.68	5.75	0.44	-	47.08	1.16	0.01	1.34	-	0.00
$(Na,Ca)_8Al_6Si_6O_{24}(I_{6.5\%},S_{100\%})_2$	7.98	26.54	37.71	8.92	0.48	0.14	15.58	1.26	0.01	1.35	-*	-
$(Na,Ca)_8Al_6Si_6O_{24}(I_{6.5\%},S_{75\%})_2$	9.05	25.77	37.46	9.08	0.09	-	14.45	1.43	0.02	1.64	-*	-
$(Na,Ca)_8Al_6Si_6O_{24}(I_{6.5\%},S_{50\%})_2$	3.20	25.72	39.75	9.99	0.00	-	17.87	1.58	0.02	1.88	-*	-

* Indicates unreliable result

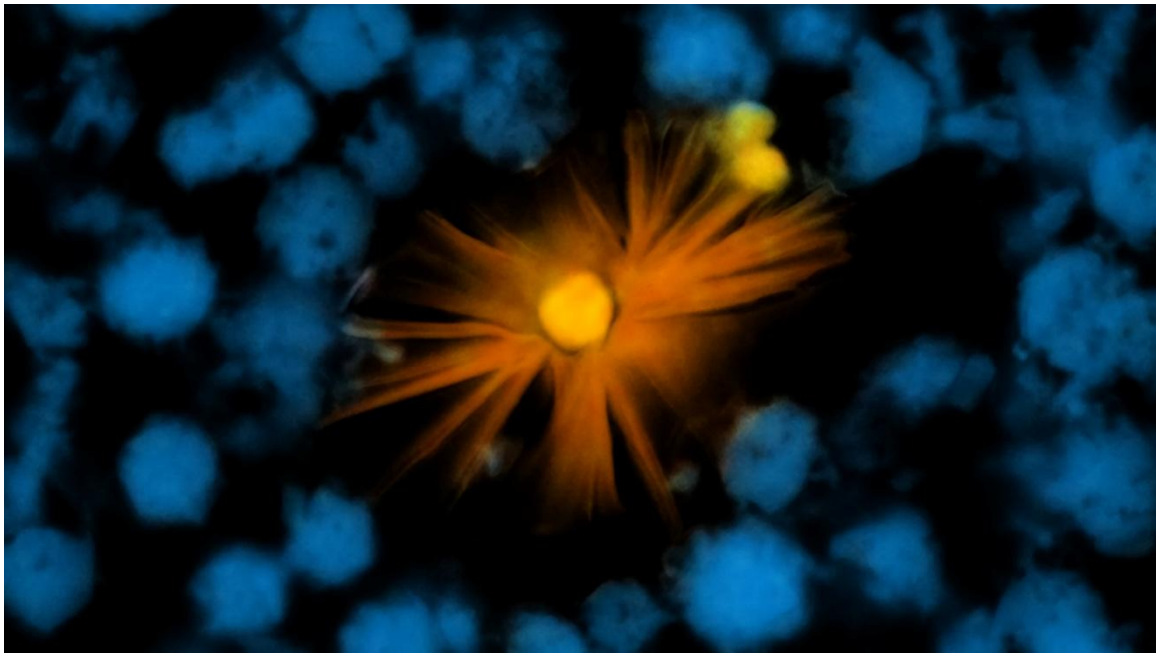

Figure S3. Enhanced SEM-EDS image of $(Na,K)_8Al_6Si_6O_{24}(I_{10\%},S_{100\%})_2$ sample, where the blue particles indicate cancrinite and the yellow Ti particle is surrounded by Mg threads.

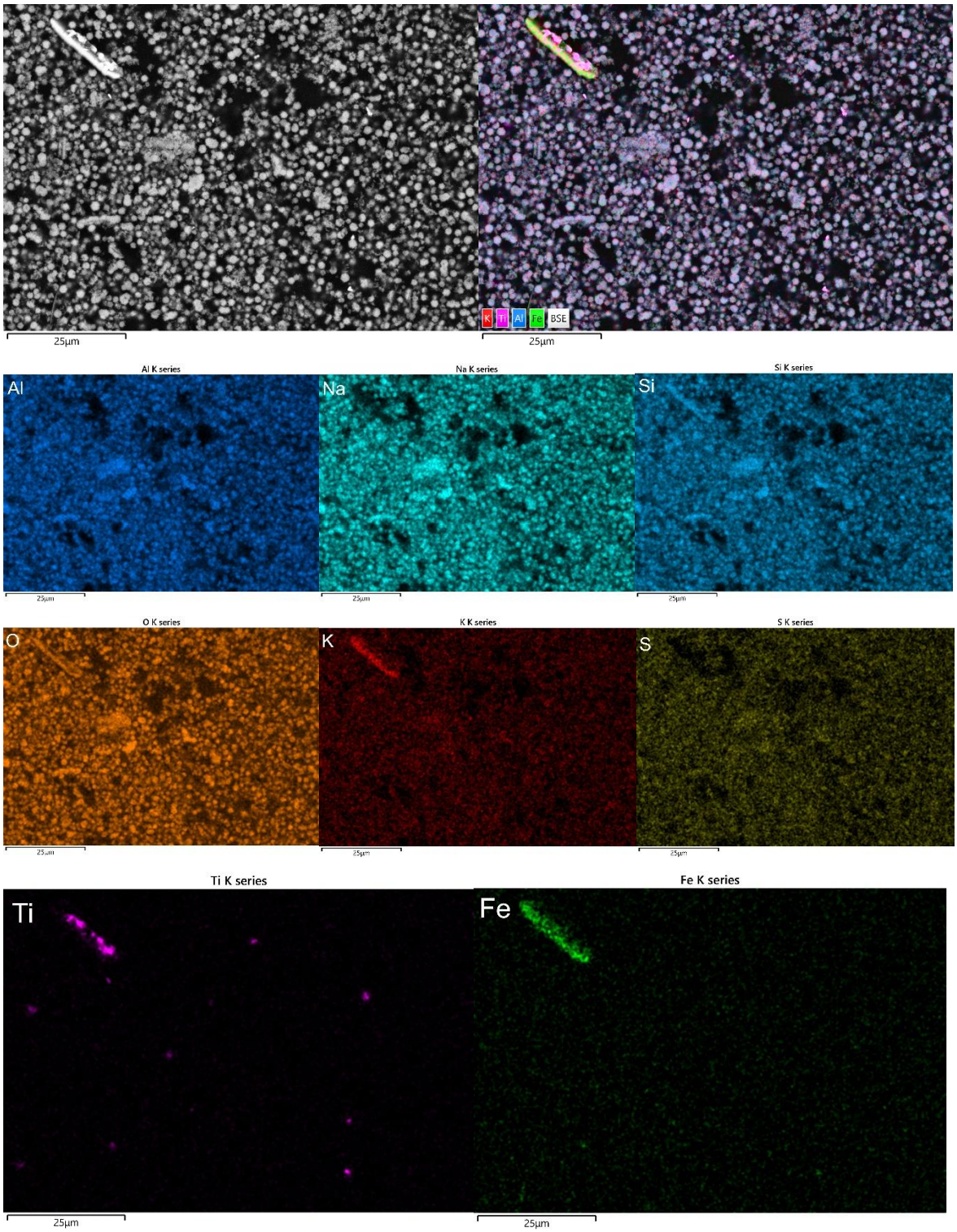

Figure S4. SEM-EDS elemental mapping with acceleration voltage of 15 kV of $(Na,K)_8Al_6Si_6O_{24}(I_{10\%},S_{100\%})_2$.

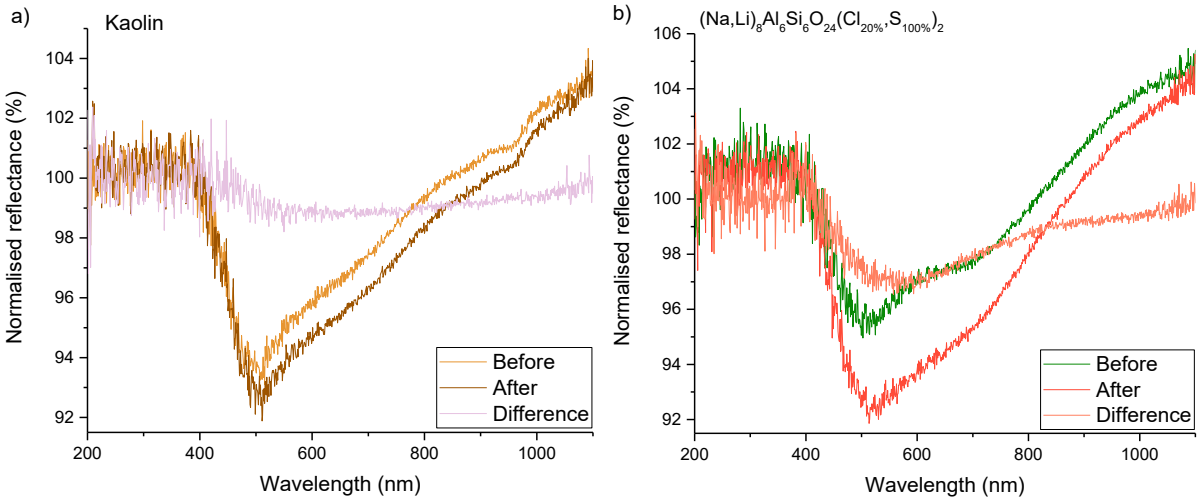

Figure S5. Reflectance spectra of a) kaolin and b) $(Na,Li)_8Al_6Si_6O_{24}(Cl_{20\%},S_{100\%})_2$ before and after irradiation with 254 nm for 5 min with the difference curve.